Doctral dissertation

博士学位論文

Clay-mineralogical features of seismogenic faults in shallow accretionary prisms: Implications to their coseismic slip behaviors

粘土鉱物学的手法を 用いた付加体浅部断層における すべり 挙動の推定

Hirokazu Masumoto

増本 広和

Department of Natural History Sciences, Graduate School of Science,

Hokkaido University

北海道大学大学院理学院 自然史科学専攻

March 2019

Abstract

Subduction zone earthquake and tsunami are serious natural hazards to people living near the coastal areas. Knowledge on the slip and propagation behaviors to shallow part of megathrust in subduction zone is important to understand tsunamigenic earthquake. In this dissertation, I applied a new temperature proxy to constrain slip parameters for the shallow branching thrust fault from the plate subduction interface (megasplay fault) recovered during the Integrated Ocean Drilling Program (IODP) Nankai Trough Seismogenic Zone Experiment (NanTroSEIZE) and a fossil imbricate thrust from a shallow part in an ancient accretionary prism (Shirako Fault, Japan).

The temperature proxy is based on the difference in susceptibility of dehydroxylation reactions of kaolinite and chlorite to heating treatment. To quantify this behavior, I carried out high-temperature X-ray diffraction (XRD) analysis and evaluated the kinetic parameters of each dehydroxylation reaction by thermogravimetric analysis using the Friedman method. For kaolinite, the thermogravimetric data are fitted with a one and a half order equation ($F_{3/2}$) with an activation energy of 171 kJ mol^{-1} and a frequency factor of 5.6×10^8 s^{-1}. The data for chlorite are analyzed by the geometrical contracting model equation (R_2) with an activation energy of 197 kJ mol^{-1} and a frequency factor of 4.5×10^9 s^{-1}.

Thermal models of frictional heating combined with the above reaction kinetics predict that repeated frictional heating can cause a selective breakdown of kaolinite relative to chlorite. Such a state is truly observed in the megasplay fault of the Nankai Trough and in the slip zone of the Shirako Fault as represented in the XRD patterns. These observations suggest that coseismic slip repeatedly propagated up

to the trench in subduction margin, and possibly triggered tsunamis.

Besides the clay dehydroxylation, the XRD analysis also revealed a local progression of the smectite-to-illite conversion (S–I) reaction in the above two fault zones. Quantitative analysis indicated that the illite content in mixed-layer illite/smectite is ~14% higher in the gouge than in the host sediments. A thermal history of the fault constrained by vitrinite reflectance analysis requires a reduction of the apparent activation energy by ~20%–30% compared with the literature value to explain the observed illitization. These results suggest that the kinetic barrier of the smectite–illite reaction is lowered as a result of mechanochemical processes in seismogenic fault zones.

概要 (Abstract in Japanese)

南海トラフなどのプレート沈み込み境界で発生する地震においては，海底近くまで達するすべり変位が生じると，それに伴う海水面の変化が津波となって周囲に伝わる可能性がある。したがって，プレート境界断層での地震性すべりが海底まで伝播しうるのかを評価することは，津波を伴う地震を理解する上で非常に重要である。本論文では，そのような断層のすべり挙動を評価するため，南海トラフ地震発生帯掘削計画 (Nankai Trough Seismogenic Zone Experiment; NanTroSEIZE) で掘削された南海トラフの巨大分岐断層と，付加体先端のインブリケート衝上断層を構成していたと考えられている房総付加体の白子断層を対象とし，断層すべり面試料 (断層ガウジ) の鉱物組成分析を行った。また，標準試料を用いた加熱実験を実施し，粘土鉱物の脱水反応を利用した新たな地質温度計を作成した。これを上述の断層試料に適用することにより，各断層における摩擦発熱の温度を求め，すべりパラメータを制約した。得られた結果は，断層に沿って付加体の先端部まで地震性高速すべりが繰り返し伝播した可能性を示唆するものであり，巨大分岐断層や付加体先端のインブリケート衝上断層は津波を伴う地震を起こしうる断層であることが明らかになった。

第 1 章では，付加体浅部断層のすべり挙動と，これまでに試みられてきた各種地質温度計を用いた断層のすべり挙動の解析例について概観する。

第 2 章では，付加体浅部を構成する堆積岩に普遍的に見られる kaolinite と chlorite を対象とし、高温 X 線回折 (X-ray diffraction; XRD) 実験と熱重量-示差熱分析 (Thermogravimetry-differential thermal analysis; TG-DTA) を行い，各鉱物の脱水反応の速度パラメータを決定した。また、各鉱物の脱水反応に伴う XRD ピーク面積の減少と反応進行度を対応付けた。

第 3 章では，南海トラフ巨大分岐断層と白子断層を対象とし，断層ガウジと

その周囲の岩石試料について定方位粉末 XRD 分析を行い，粘土鉱物組成や混合層構造の検討を行った。その結果、断層ガウジにおいて，kaolinite の脱水反応の進行が見られた。そこで，2 章で得られた粘土脱水反応の速度パラメータに基づいて各断層における温度履歴を評価した。すべり速度，摩擦係数、すべり継続時間を変化させて摩擦発熱に伴う断層帯の温度発展を計算し，各イベントにおける kaolinite と chlorite の脱水反応進行度を計算した。その結果，南海トラフの巨大分岐断層では 1 回の地震イベントを仮定すればおよそ 420–470 ℃の範囲の温度上昇で kaolinite の選択的分解が進行することが示された。反応進行における発熱作用の繰り返しの効果も検討したところ，イベントが 10 回の繰り返しであれば断層帯の最高到達温度は約 370–420 ℃, 100 回であれば約 330–380 ℃の温度が見積もられた。一方，先行研究によるビトリナイト反射率を用いた解析により、巨大分岐断層ガウジの最高到達温度は約 330 ℃と見積もられている。この先行研究の結果をあわせると，断層では粘土鉱物の反応は室内実験で得られた結果より低い温度で進んでいるか，イベントの繰り返しの積分をみている可能性がある。一方，白子断層においては，イベントの繰り返しを考慮することで先行研究と矛盾しない摩擦発熱温度 (約 410–470 ℃) が得られた。これらの結果は，沈み込み帯浅部の大規模逆断層では，地震性すべりが海底付近まで普遍的に伝播することを示唆する。

第 4 章では，断層におけるイライト -スメクタイト混合層鉱物のイライト化反応を対象とし，摩擦すべりに伴うメカノケミカル作用が反応に及ぼす影響について検討した。まず南海トラフ巨大分岐断層試料について，XRD による混合層鉱物の構造評価を行った。その結果，巨大分岐断層では有意なイライト化反応の進行が確認された。また，ビトリナイト反射率測定から求められた熱履歴に基づき，既存のイライト化反応速度式を用いて断層内の反応進行を計算したところ，観察された反応を再現できないことが分かった。これは，断層すべりに伴うメカノケミカル作用により，イライト化反応が静的な環境よりも進みやすくなっている可能性を示唆している。そこで，イライト化反応速度式の活性化エネルギーを変化させ，反応の再現を試みた。その結果，活性化エネルギーを約 30%減少させると巨大分岐断層でのイライト化反応を再現できることがわかった。また，白子断層においても同様の解析を行ったところ，活性化エネルギーを約 20%減少させるとイライト化反応を再現できた。以上の結果は，地震

性すべりによるメカノケミカル作用によって，断層内の各種反応が促進される可能性を示唆している。このことはまた、断層の熱履歴解析に地質温度を適用する際には，速度式を適切に較正する必要があることを示している。

Acknowledgements

Firstly, I wish to express my sincere gratitude to my supervisor Dr. Jun Kameda who gave many advices, encouragement, and financial support during this research in Hokkaido university. I would like to thank co-supervisor, Dr. Toru Takeshita, for his great support.

I would like to thank Dr. Kazumasa Sugiyama and Dr. Hiroshi Arima for giving the opportunity to carry out high-temperature XRD experiments at Institute for Materials Research, Tohoku University. I also acknowledge financial support for travel from Tohoku University. I would like the thank Dr. Takaya Nagai for giving the opportunity to use XRD and TG-DTA. I am grateful to him for helpful suggestion during my work. I also wish to thank Dr. Yuzuru Yamamoto for assisting me during fieldwork in the Boso peninsula. I would like to acknowledge Dr. Kohtaro Ujiie and Dr. Yujin Kitamura for kindly providing the core samples of site C0004 from NanTroSEIZE.

Many people in my department have discussed about my work with me: Dr. Jin'ichiro Maeda, Dr. Makoto Kawamura, and Dr. Marie Python. I wish to thank them for their constructive suggestions. Thanks also to Ms. Megumi Mori for technical support during the XRD measurement using Rigaku SmartLab at the Open Facility of Hokkaido University Sousei Hall.

Contents

List of Tables

List of Figures

Chapter 1

Introduction

1.1 Previous attempts for quantitative estimation of frictional heating during coseismic slip

Subduction zone earthquake and tsunami are serious natural hazards to people living near the coastal areas. Knowledge on the slip and propagation behaviors to shallow part of megathrust in subduction zone is important to understand tsunamigenic earthquake. During the 2011 Tohoku-Oki earthquake (moment magnitude M_w 9.0), the coseismic displacement of ~50–80 m had reached the axis of the Japan Trench (Fujiwara et al., 2011; Ito et al., 2011), resulted in destructive tsunami. Along the Nankai trough subduction margin in southwest Japan, where a modern accretionary prism is formed as a result of the Philippine Sea Plate subduction beneath the Eurasian plate, large earthquakes and accompanying tsunamis repeatedly occurred (e.g. Ando, 1975). To investigate the generation mechanism of the Nankai Trough earthquakes, the International Ocean Drilling Program (IODP), Nankai Trough Seismogenic Zone Experiments (NanTroSEIZE), was started in 2007, and have drilled deep holes along the transect off the Kii peninsula and recovered core samples from the megasplay fault and the frontal décollement.

Seismic slip generates frictional heat on the slip plane. Most distinctive record

of frictional heating is pseudotachylyte, a product of fault rock melting during faulting (e.g. Sibson, 1975). Recently, growing numbers of pseudotachylyles have been found in accretionary prisms (e.g. Ikesawa et al., 2003; Mukoyoshi et al., 2006; Rowe et al., 2005; Ujiie et al., 2007). Concurrently, efforts have been made to assess the process with a moderate temperature increase (less than melting temperatures of rock-forming minerals). Geothermometers are often used for such purposes, and several proxies have been proposed so far. Based on vitrinite reflectance geotehrmometry, O'Hara (2004) found temperature anomaly along the slip zones of the faults in the eastern Kentucky and Montana (USA), and in the south Wales coalfield (UK). Sakaguchi et al. (2011) also reported vitrinite reflectance anomaly along the megasplay fault and the frontal décollement in the Nankai trough.

Since the pioneering work of Ishikawa et al. (2008), trace elements geochemistry has been used for detecting coseismic high-temperature fluid-rock interactions in the various faults; the Chelungpu fault in Taiwan (Ishikawa et al., 2008), the Miura-Boso accretionary prism (Hamada et al., 2011; Hirono & Ishikawa, 2018), an out-of-sequence thrust fault in the Shimanto accretionary complex (Honda et al., 2011), and the black fault rocks in the Kodiak accretionary complex (Yamaguchi et al., 2014). Magnetic mineral analyses are also used for detecting temperature anomaly in fault based on formation of magnetic minerals from paramagnetic minerals (Mishima et al., 2006, 2009).

More recently, biomarkers (Polissar et al., 2011; Rabinowitz et al., 2017; Savage et al., 2014; Sheppard et al., 2015) and Raman spectroscopy of carbonaceous material (Hirono et al., 2015; Kaneki et al., 2016; Mukoyoshi et al., 2018) have attracted much attention as effective geothermometers.

1.2 Clay minerals behaviors at elevated temperatures

Clay minerals are hydrous layer silicates and part of the family of phyllosilicates (e.g. Bailey, 1980). They are major components of shallow crustal faults and

can greatly control the frictional behaviors (e.g. Ikari et al., 2009; Takahashi et al., 2009). As mentioned above, coseismic slip has potential to raise fault zone temperature by frictional heating. In this study, I especially focus on two thermally-activated processes of clay minerals, dehydroxylation and conversion reaction, triggered by frictional heating.

Many researches have determined kinetic parameters of the dehydroxylation reactions of illite (e.g. Gualtieri & Ferrari, 2006; Hirono & Tanikawa, 2011), smectite (e.g. Girgis et al., 1987; Güler & Sarier, 1990; Levy & Hurst, 1993; Murray & White, 1949, 1955) and kaolinite (e.g. Brindley & Nakahira, 1957; Criado et al., 1984; Levy & Hurst, 1993; Ortega et al., 2010). However, dehydroxylation of chlorite is poorly understood. Hirono et al. (2008) and Kuo et al. (2009, 2011) documented dehydroxylation of clay minerals within the slip zone of the Taiwan Chelungpu fault possibly caused by frictional heating during the 1999 Chi-Chi earthquake.

Mixed-layering is a typical structural variability in layered materials where two or more kinds of unit layers pile up in a vertical stacking sequence (e.g. Reynolds, 1980; D. M. Moore & Reynolds, 1997). Illite-smectite mixed-layer is a common phase in in sedimentary basins (e.g. Burst Jr., 1957; Hower et al., 1976; Perry & Hower, 1970). With increase of diagenetic grade, illite content in the mixed-layer successively increases (i.e., smectite to illite conversion (S–I)). The local progression of the S–I reaction within the fault gouge was observed along a fossil imbricate thrust in the Miura-Boso accretionary prism (Kameda et al., 2013). Yamaguchi et al. (2011) also reported the illitization reaction in the dark gouge along a megasplay fault in the Nankai Trough. These findings suggest that the reaction can be fostered even by a transient process such as frictional heating.

1.3 Motivation

As mentioned above, there are several previous works aiming at quantifying slip behavior of the sesimogenic faults using geothermometers. Given the universality and predominance of clay minerals at shallow crustal levels, application of reaction

kinetics of clay minerals is thought as an effective geothermometer of the fault hosted in sedimentary rocks such as tsunamigenic fault in subduction zone.

The aims of this dissertation are:

1. To develop a new temperature proxy using dehydroxylation reaction of clay minerals. To this end, I evaluate kinetic parameters of dehydroxylation reaction of kaolinite and chlorite by thermogravimetric analysis (Chapter 2). In Chapter 3, I use this method to estimate experienced temperature of the shallow subduction zone thrust faults (the Shirako Fault in the Miura-Boso accretionary prism and the Nankai trough megasplay fault).

2. To evaluate mechanochemical effect on reaction kinetics of clay minerals within seismogenic faults. In Chapter 4, I examine the conversion reaction of smectite to illite within the above two fault zones as typical examples of this issue. Based on the results, I propose a new kinetic expression of the S–I conversion reaction.

Chapter 2

Dehydroxylation kinetics of kaolintie and chlorite

2.1 Introduction

High-velocity coseismic slip causes transient temperature rise in a fault zone due to frictional heating (e.g. Scholz, 1980; Sibson, 1977). Analysis of such temperature record is a key to understanding earthquake mechanics. Many studies have attempted to quantify frictional heating events on ancient or active faults by using temperature proxies such as vitrinite reflectance (e.g. Hamada et al., 2015; O'Hara, 2004; Sakaguchi et al., 2007, 2011), trace element geochemistry (e.g. Hamada et al., 2011; Honda et al., 2011; Ishikawa et al., 2008), biomarkers (Polissar et al., 2011; Rabinowitz et al., 2017; Savage et al., 2014; Sheppard et al., 2015), and Raman spectroscopy of carbonaceous material (Hirono et al., 2015; Kaneki et al., 2016; Mukoyoshi et al., 2018). Dehydroxylation of clay minerals has been also examined to constrain the slip behavior of the fault (Hirono et al., 2008; Kuo et al., 2009). After the Chi-Chi earthquake in 1999, the Taiwan Chelungpu Fault Drilling Project recovered slip zone materials from two drill holes (Holes A and B; Ma et al., 2006). Hirono et al. (2008) and Kuo et al. (2009) noted the absence of kaolinite and chlorite peaks in the X-ray diffraction (XRD) patterns for samples from the principal slip zone on the Chelungpu Fault, suggesting that these clay minerals

decomposed due to dehydroxylation at elevated temperatures. Kuo et al. (2011) estimated the temperature conditions of the slip zones by conducting isothermal heating experiments on the core samples, concluding that the temperature in one particular sample of black gouge (FZ1111; principal slip zone) was raised to 900 °C–1100 °C, whereas another (FZ1153) had experienced temperatures of only 500 °C–900 °C, because within it kaolinite had broken down, but illite and chlorite peaks were still present. However, their approach may have underestimated the temperature during coseismic slip because the heating experiments were conducted at a heating rate of 150 °C, which is much slower than the rate of frictional heating expected in natural fault zones (~10^1–10^2 °C s^{-1}; Rowe & Griffith, 2015).

Since kaolinite and chlorite are common constituent minerals in fault zones at subduction margins, investigation of the reaction kinetics of their dehydroxylation reactions may be able to provide more insights into the slip behavior along such faults. For example, Kameda et al. (2013) investigated the clay mineralogy of a slip zone in an ancient accretionary complex (Shirako Fault, Japan), which is thought as an on-land analog of the shallow branching fault in the Nankai accretionary margin (Yamamoto et al., 2005), and found a reduction in the XRD peak intensity of kaolinite relative to chlorite within the slip zone (Figure 2.1; Table 2.1). The authors interpreted this observation as a result of frictional heating on this fault, but they failed to constrain the temperature condition due to lack of knowledge of how the XRD peak intensities of kaolinite and chlorite change in response to the thermal decomposition and dehydroxylation. In general, the kinetic parameters for dehydroxylation of clay minerals can be determined by thermogravimetric analyses. However, the reacted fraction of dehydroxylation is not necessarily equal to the fractional change of the XRD peak intensity. Therefore, the kinetic parameters obtained are not easily applied in interpretation of XRD results from the natural fault zone samples. One way we could link these properties is to perform high-temperature XRD measurements on the clay samples to demonstrate how the patterns change at elevated temperatures, and to estimate the dehydroxylation state of the heated samples by kinetic calculation of a given

temperature–time path during the experiment.

Many studies have examined the kinetics of kaolinite dehydroxylation (e.g. Brindley & Nakahira, 1957; Criado et al., 1984; Levy & Hurst, 1993; Ortega et al., 2010; Tsuzuki & Nagasawa, 1957), whereas little research has focused on the kinetics of chlorite dehydroxylation. An exception is the study by Tsuzuki and Nagasawa (1957), who determined the kinetic parameters for the dehydroxylation reactions of chlorite and other hydrous minerals by isothermal heating experiments using a thermobalance. However, they did not take account of the fact that chlorite dehydroxylation occurs in two stages (Brindley & Ali, 1950; Brindley & Chang, 1974; Caillère & Hénin, 1957; Grim, 1968), which requires more systematic analyses for the accurate determination of the kinetic parameters of chlorite.

To develop a new proxy to constrain parameters of earthquake slip for fault zones containing kaolinite and chlorite, we performed three experiments as follows: (1) high-temperature XRD experiments to investigate how the XRD patterns of kaolinite and chlorite change due to dehydroxylation at elevated temperatures; (2) thermogravimetric analyses to determine the kinetic parameters for each dehydroxylation reaction, and application of these parameters to estimate the dehydroxylation state of the samples analyzed using XRD.

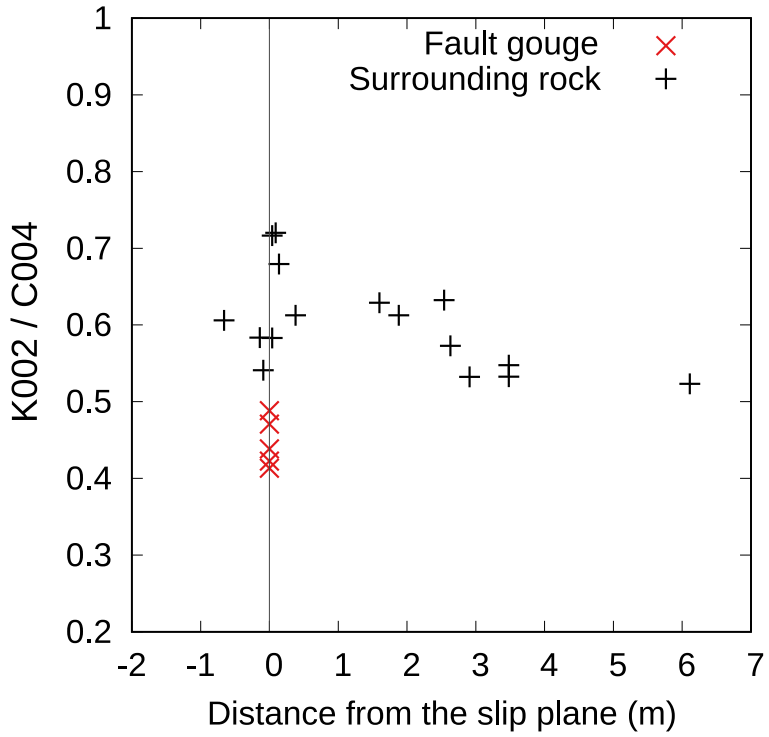

Figure 2.1: XRD peak area ratio of kaolinite 002 to chlorite 004. The results are taken from Kameda et al. (2013). The decrease in kaolinite 002 / chlorite 004 can be explained by the decrease in kaolinite peak intensity (Kameda et al., 2013).

Table 2.1: XRD analyses results from the Shirako Fault by Kameda et al. (2013).

Sample name	Distance from the slip zone (m)	Rock type	K002			C004			K002/C004	Normalized K002/C004
			Position	Area	FWHM	Position	Area	FWHM		
SRK01	2.91	Intact siltstone	24.85	10996	0.230	25.11	20655	0.268	0.53	0.88
SRK02	3.48	Intact siltstone	24.84	8644	0.235	25.11	15787	0.277	0.55	0.91
SRK03	0.38	Intact siltstone	24.87	11782	0.270	25.12	19231	0.262	0.61	1.02
SRK04	1.6	Intact siltstone	24.85	18354	0.282	25.11	29182	0.273	0.63	1.05
SRK05	2.63	Intact siltstone	24.83	13685	0.276	25.10	23891	0.285	0.57	0.95
SRK06	3.48	Intact siltstone	24.85	12466	0.246	25.11	23402	0.272	0.53	0.89
SRK07	1.88	Intact siltstone	24.85	10270	0.242	25.11	16765	0.254	0.61	1.02
SRK08	2.54	Intact siltstone	24.87	11092	0.273	25.13	17537	0.261	0.63	1.05
SRK09	−0.66	Intact siltstone	24.86	10805	0.262	25.12	17830	0.268	0.61	1.01
SRK10	6.11	Intact siltstone	24.86	13256	0.261	25.12	25335	0.284	0.52	0.87
SRK11	0.04	Breccia	24.86	7162	0.218	25.13	12285	0.271	0.58	0.97
SRK11a	0.04	Breccia	24.87	4930	0.282	25.14	6880	0.253	0.72	1.19
SRK12	−0.14	Intact siltstone	24.87	7748	0.278	25.14	13279	0.262	0.58	0.97
SRK13	0.09	Intact siltstone	24.88	15075	0.306	25.14	20931	0.272	0.72	1.20
SRK14	−0.09	Intact siltstone	24.85	7989	0.244	25.12	14766	0.280	0.54	0.90
SRK15	0.14	Intact siltstone	24.86	6451	0.275	25.12	9495	0.275	0.68	1.13
Average					0.261			0.270	0.60	1.00
2σ									0.12	0.20
FG01a	0	Fault gouge	24.87	4028	0.226	25.12	9188	0.234	0.44	0.73
FG01b	0	Fault gouge	24.85	5857	0.214	25.11	14172	0.260	0.41	0.69
FG01c	0	Fault gouge	24.87	5436	0.204	25.12	12862	0.253	0.42	0.70
FG02a	0	Fault gouge	24.88	9453	0.259	25.13	19360	0.245	0.49	0.81
FG02b	0	Fault gouge	24.86	8358	0.231	25.11	17755	0.257	0.47	0.78
Average					0.227			0.250	0.45	0.74
2σ									0.06	0.09

2.2 Materials and methods

2.2.1 Samples

Kaolinite and chlorite standard samples were obtained from the Clay Minerals Society (USA; http://www.clays.org/). These are a well-ordered kaolinite ($Al_4Si_4O_{10}(OH)_8$; KGa-1B from Buffalo China Mine, Washington County, Georgia, USA; Pruett & Webb, 1993) and Fe-bearing chlorite ripidolite ($(Mg_{5.54}Fe^{2+}_{3.02}Fe^{3+}_{0.94}Al_{2.48})[Si_{5.33}Al_{2.66}]O_{20}(OH)_{16}$; CCa-2 from Flagstaff Hill, El Dorado County, California, USA; Post & Plummer, 1972; Brandt et al., 2003). The unit-cell parameters for kaolinite and chlorite CCa-2 have been reported in previous studies: kaolinite with triclinic $C1$ crystal structure, a = 5.1554 Å, b = 8.9448 Å, c = 7.4048 Å, α = 91.700°, β = 104.862°, γ = 89.822° (Bish & von Dreele, 1989); chlorite CCa-2 with monoclinic space group $C2/m$, a = 5.35 Å, b = 9.27 Å, c = 14.26 Å, β = 97.33° (Gailhanou et al., 2009). Both were dispersed in distilled water, and each sample under 2 µm in spherical equivalent size was subsequently separated with a centrifuge according to Stokes' law and employed for the following analysis.

2.2.2 High-temperature X-ray diffraction experiments

High-temperature XRD experiments allowed examination of the crystallographic behavior of kaolinite and chlorite at elevated temperatures. Suspensions of a 1:1 mixture of kaolinite and chlorite were dropped onto an α-alumina substrate, then air dried in an oven at 60 °C. The XRD experiments were performed at temperatures from 298 K (25 °C) to 973 K (700 °C) using a Rigaku RINT-Ultima III X-ray diffractometer equipped with a pyloritic graphite monochrometer in the diffracted beam path. The X-ray diffraction profiles were measured with Cu$K\alpha$ radiation in the step scan mode (5-s exposure per 0.01°). The temperature conditions during the experiments were calibrated using thermal expansion of the standard MgO sample (Touloukian et al., 1977). The sample chamber of the instrument was purged with high-purity N_2 at a rate of 200 $cm^3\,min^{-1}$. XRD

patterns of the samples at 2θ = 11.5°–13.0° for the composite peak of kaolinite 001 + chlorite 002 (hereafter termed "K001 + C002") and 24.0°–26.0° for kaolinite 002 + chlorite 004 (hereafter termed "K002 + C004") were obtained at 298, 373, 473, 573, 623, 673, 723, 773, 823, 873, 923, and 973 K (25, 100, 200, 300, 350, 400, 450, 500, 550, 600, 650, and 700 °C). The temperature was raised between these conditions at a rate of 10 K min^{-1} and was held constant during the measurements. Two sets of high-temperature experiments were conducted to confirm the reproducibility of the analyses. Peak profile analysis was carried out using Macdiff (version 4.2.6) software developed by Petschick (2010). This software smoothes profiles, calculates baselines, corrects angle using the peak of α-alumina at 298 K, decomposes the peaks based on the Pearson-type VII function, and measures the integrated peak intensity and full width at half maximum (FWHM) of individual peaks.

2.2.3 Thermal analysis and determination of Kinetic parameters

Thermogravimetric (TG) analysis and differential thermal analysis (DTA) were performed in order to determine the reaction mechanisms and kinetic parameters for dehydroxylation reactions of kaolinite and chlorite. TG, derivative TG (DTG), and DTA curves were obtained using a Rigaku Thermo Plus EVO TG8120 thermal analyzer. Approximately 10 mg of the sample was heated in a Pt cup at a rate of 10 K min^{-1} up to 393 K (120 °C), and then held at 393 K for 30 min to remove adsorbed water. The samples were then heated to 1473 K (1200 °C) at constant rates of 2, 5, 10, 20, and 40 K min^{-1} under N_2 flowing at a rate of 100 cm^3 min^{-1}.

The apparent activation energy (E_a) was estimated based on the Friedman (1964) method, which yields E_a corresponding to the reaction mechanism. The reacted fraction α can be expressed as

$$\alpha = \frac{w_t - w_0}{w_f - w_0} \tag{2.1}$$

where w_t, w_0, and w_f are the weight at time t, the initial weight, and the final weight, respectively. The kinetic equation of a chemical reaction is expressed as

$$\frac{d\alpha}{dt} = kf(\alpha) \tag{2.2}$$

where k is the reaction rate and $f(\alpha)$ is the differential form of the kinetic expression. The temperature dependence of the reaction rate is described by the Arrhenius equation:

$$k = A\exp\left(-\frac{E_a}{RT}\right) \tag{2.3}$$

where A is the frequency factor, E_a is the apparent activation energy, R is the gas constant ($8.314\,\mathrm{J\,K^{-1}\,mol^{-1}}$), and T is the temperature (in K). Therefore, the kinetic equation can be expressed as

$$\frac{d\alpha}{dt} = A\exp\left(-\frac{E_a}{RT}\right) f(\alpha) \tag{2.4}$$

and the natural logarithm of equation (2.4) is

$$\ln\frac{d\alpha}{dt} = -\frac{E_a}{RT} + \ln(A) + \ln[f(\alpha)]. \tag{2.5}$$

The apparent activation energy E_a can then be determined by plotting $\ln\frac{d\alpha}{dt}$ versus $\frac{1}{T}$ for each activation energy. To determine the reaction mechanism and frequency factor, integration of equation (2.4) gives

$$\int_0^\alpha \frac{d\alpha}{f(\alpha)} = A\int_0^t \exp\left(-\frac{E_a}{RT}\right) dt \tag{2.6}$$

$$g(\alpha) = A\Theta \tag{2.7}$$

where $g(\alpha)$ is an integral form of the conversion function equal to $\int_0^\alpha \frac{d\alpha}{f(\alpha)}$ and Θ is the reduced time that is equal to $\int_0^t \exp\left(-\frac{E_a}{RT}\right) dt$ (Ozawa, 1965, 1970, 1986). Θ was obtained using a numerical integration of the TG data. The reaction mechanism was then able to be determined by analyzing a linear regression for $g(\alpha)$ versus Θ using the least squares method, with the slope

of the plot yielding the frequency factor A. Kinetic expressions of solid-state reactions are taken from Šesták and Berggren (1971) and Khawam and Flanagan (2006). To estimate the dehydroxylation state of the heated samples during XRD measurements, we calculated the integrated fraction of dehydroxylation reaction using kinetic parameters determined above for the temperature–time path during the experiments.

2.3 Results

Figure 2.2 shows XRD profiles from 25 °C to 600 °C; the peak positions for K001 and K002 gradually shifted to lower angles with increasing temperature, implying that thermally driven crystal expansion occurred along [001]. The corresponding peak intensities of K001 and K002 start to decrease above 400 °C, and fully disappear at 500 °C. No significant change was observed with respect to C002 and C004 peaks up to 500 °C, but the peaks of chlorite suddenly disappear at 550 °C. The shape of K001 + C002 peak shows similar trend to K002 + C004. Here we choose K002 + C004 for peak decomposition because the 2θ angle between K002 and C004 is broader than between K001 and C002. K002 + C004 peak can easily be decomposed from XRD data even at the room temperature. The integrated intensity of K002 and C004 normalized by the starting value and the intensity ratio of K002/C004 typically show an inverse dependence on temperature (Figure 2.3). The results of decomposition behavior for K002 and C004 are summarized in Table 2.2.

The measured TG curves for kaolinite show one stage of weight loss by dehydroxylation (Figure 2.4a), whereas the TG curves for chlorite demonstrate two stages of dehydroxylation (Figure 2.4b), consistent with previous studies by Brindley and Ali (1950), Caillère and Hénin (1957), Grim (1968), and Brindley and Chang (1974). The two stages of dehydroxylation occur within the brucite layer at lower temperatures (~500–600 °C) and the talc-like 2:1 layers at higher temperatures (~700–800 °C). The DTG and DTA results are also shown in Figures 2.5 and 2.6. We have evaluated the kinetic parameters for the dehydroxylation of kaolinite and the earlier stage of chlorite dehydroxylation associated with

the decomposition of the brucite layer and demonstrate this using a Friedman plot (Figure2.7; Friedman, 1964) for the dehydroxylation of kaolinite and chlorite, where the data are fitted by slopes equal to $-\frac{E_a}{R}$. The Friedman (1964) method indicates that the apparent activation energies for kaolinite and chlorite dehydroxylation in our study are 171 and 197 kJ mol^{-1}, respectively (Table 2.3). Fitting results with the above parameters for different reaction mechanisms (Table 2.4) indicate that our TG data are best fit by a one and a half order equation ($F_{3/2}$) for kaolinite KGa-1B and the geometrical contracting model equation (R_2) for chlorite CCa-2. Frequency factors were determined to be 5.6×10^8 s^{-1} for KGa-1B and 4.5×10^9 s^{-1} for CCa-2.

We estimated the reacted fraction during the high-temperature XRD experiments from 300 °C to 600 °C using numerical methods (Figure 2.8). The high-temperature XRD experiments demonstrate that selective collapse of kaolinite had completed at the end of the 450 °C measurement (Figure 2.3a), while the process should have started somewhere during the 400 °C measurement. We conservatively adopted its beginning as the start of the process. The integrated fraction of kaolinite dehydroxylation at these two end member elapsed times was estimated to be 0.10 and 0.67. In contrast, chlorite dehydroxylation had only progressed by less than 0.14 by the end of this time interval. The dehydroxylated fraction of kaolinite and chlorite reached ~0.97 and ~0.86, respectively, by the time the temperature condition was finished at 500 °C.

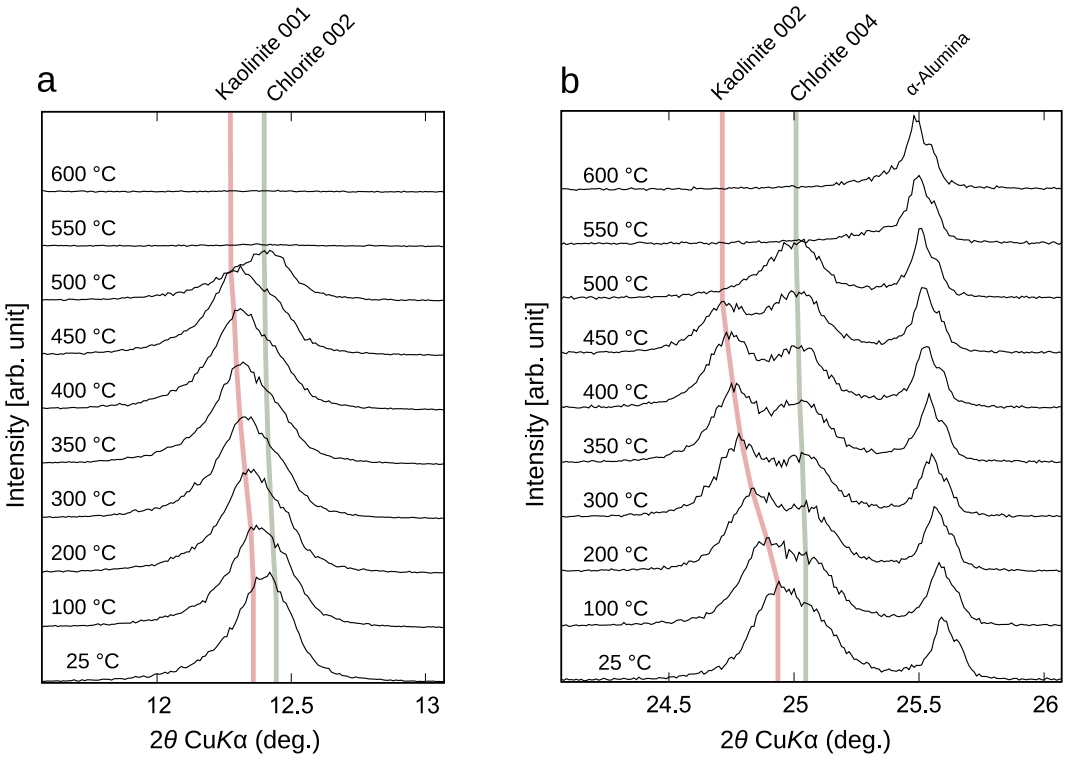

Figure 2.2: High-temperature XRD patterns for kaolinite and chlorite (second run) for the 2θ range of (a) 11.6°–13.1° and (b) 24.1°–26.1°.

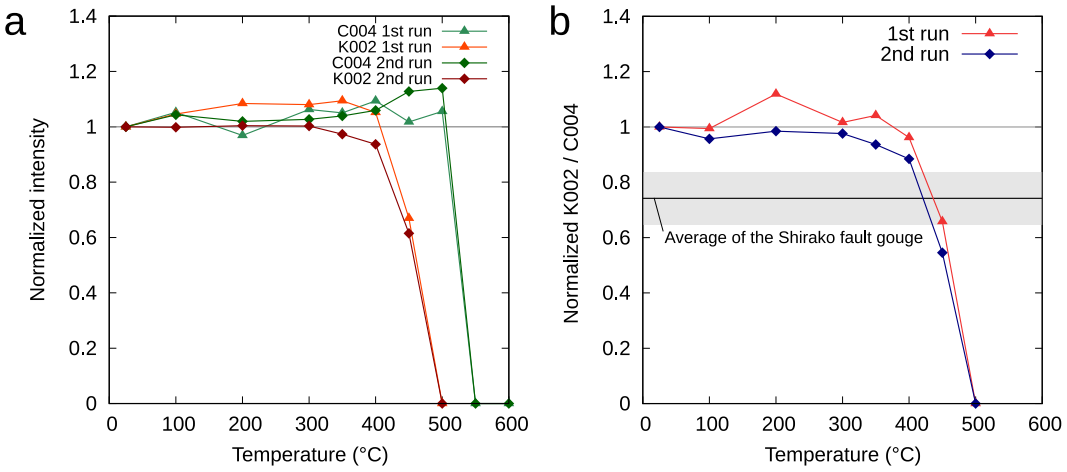

Figure 2.3: Changes in (a) the integrated intensity of K002 and C004 peaks and (b) the normalized K002/C004. Results for the fault gouge in the Shirako Fault (Kameda et al., 2013) are also shown. The shaded area shows the standard deviation ($\pm 2\sigma$).

Table 2.2: Results of peak decomposition analyses for K002 and C004.

	K002			C004			K002/C004	Normalized
Temperature (°C)	Position	Area	FWHM	Position	Area	FWHM		K002/C004
First run								
25	24.93	499	0.182	25.09	575	0.203	0.87	1.00
100	24.88	522	0.206	25.09	605	0.235	0.86	0.99
200	24.85	541	0.226	25.08	557	0.243	0.97	1.12
300	24.77	539	0.237	25.05	611	0.279	0.88	1.02
350	24.76	546	0.240	25.05	604	0.275	0.90	1.04
400	24.75	525	0.218	25.04	629	0.274	0.83	0.96
450	24.74	334	0.251	25.04	585	0.275	0.57	0.66
500	—	0	—	25.02	607	0.256	0	0
550	—	0	—	—	0	—	—	—
600	—	0	—	—	0	—	—	—
650	—	0	—	—	0	—	—	—
700	—	0	—	—	0	—	—	—
Second run								
25	24.92	3146	0.213	25.08	2691	0.255	1.17	1.00
100	24.88	3141	0.209	25.07	2808	0.239	1.12	0.96
200	24.83	2807	0.213	25.05	3115	0.258	0.90	0.77
300	24.79	3155	0.239	25.05	2764	0.264	1.14	0.98
350	24.76	3062	0.233	25.04	2797	0.268	1.09	0.94
400	24.74	2948	0.232	25.03	2851	0.267	1.03	0.88
450	24.72	1935	0.242	25.02	3035	0.275	0.64	0.55
500	—	0	—	25.02	3067	0.277	0	0
550	—	0	—	—	0	—	—	—
600	—	0	—	—	0	—	—	—
650	—	0	—	—	0	—	—	—
700	—	0	—	—	0	—	—	—

Table 2.3: Activation energies and frequency factors for the dehydroxylation of kaolinite KGa-1B and the brucite layer in chlorite CCa-2.

Reacted fraction α	Kaolinite, KGa-1B E_a (kJ mol^{-1})	Chlorite, CCa-2 E_a (kJ mol^{-1})
0.2	171	184
0.3	162	199
0.4	170	198
0.5	169	194
0.6	174	194
0.7	174	194
0.8	178	196
0.85	170	201
Average	171	197

2.4 Discussions

Our high-temperature XRD experiments confirm that kaolinite breaks down selectively over a restricted temperature range. K001 and K002 peaks start to disappear from 400 °C to 450 °C (Figure 2.2), but C002 and C004 peaks are observed up to 500 °C (Figures 2.2 and 2.3), implying that K002/C004 values start to decrease from 400 °C to 450 °C. Considering short-lived and transient heating in natural fault zones, this result suggests that the fault gouge experienced temperatures of at least 400–450 °C.

Kinetic parameters for the dehydroxylation of kaolinite and chlorite were determined in order to evaluate the temperature experienced during an earthquake slip event more robustly. For kaolinite, we obtained a one and a half order equation ($F_{3/2}$) with an activation energy of 171 kJ mol^{-1} and a frequency factor of 5.6×10^8 s^{-1} from the thermogravimetric data. This activation energy is consistent with previous studies of KGa-1 (163 kJ mol^{-1} from Levy and Hurst (1993) and 167 kJ mol^{-1} from Bellotto et al. (1995)). For chlorite, the geometrical contracting model equation (R_2) with an activation energy of 197 kJ mol^{-1} and a frequency factor of 4.5×10^9 s^{-1} yielded a reasonable fit to the thermogravimetric data for the earlier stage of dehydroxylation. A decrease in the C004 peak below 550 °C could be associated with brucite layer dehydroxylation (e.g. Guggenheim & Zhan, 1999; Villiéras et al., 1994, 1993; Zhan & Guggenheim, 1995). The kinetic parameters we

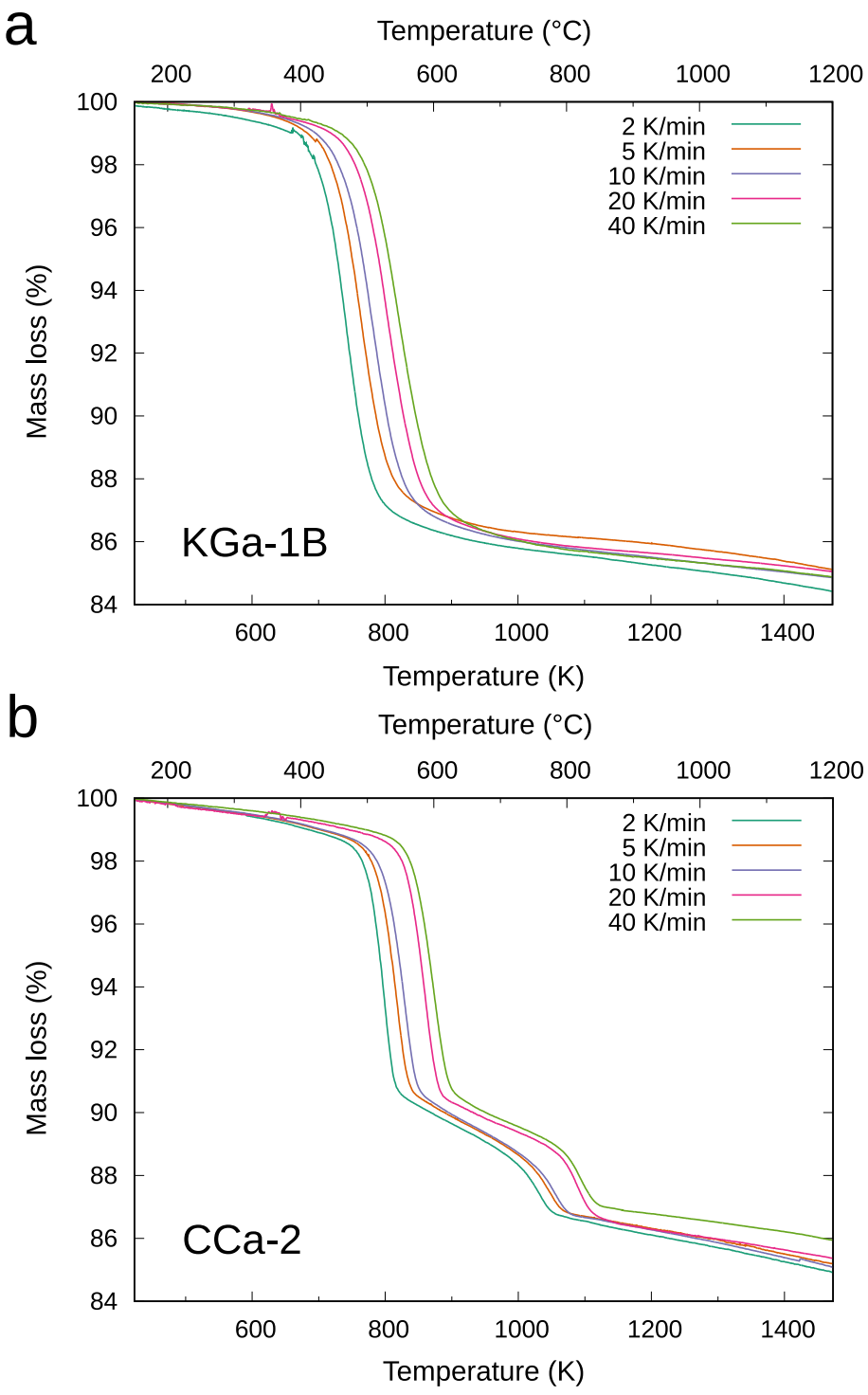

Figure 2.4: Results of thermogravimetric analysis of (a) kaolinite KGa-1B and (b) chlorite CCa-2.

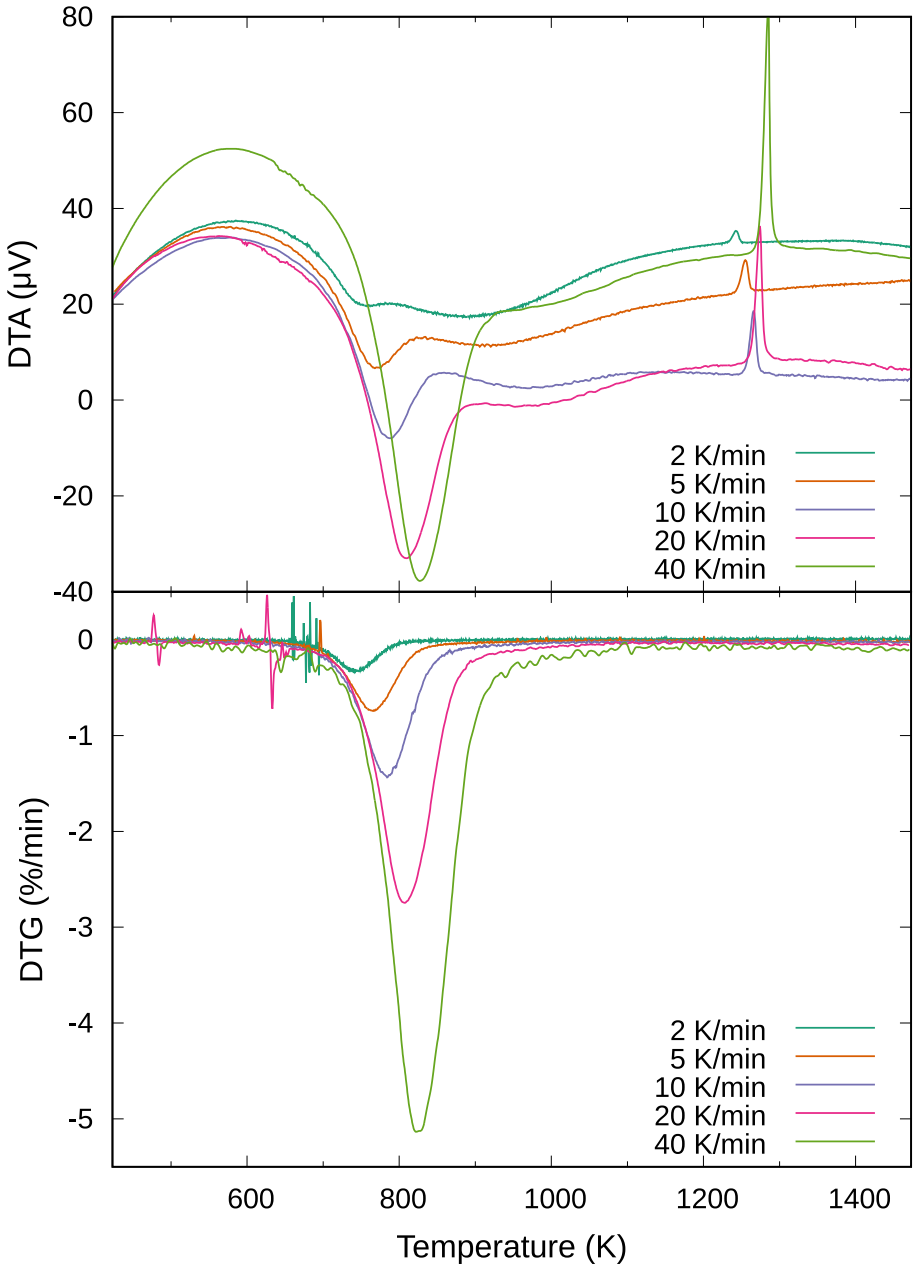

Figure 2.5: DTG and DTA results of dehydroxylation of kaolinite KGa-1B.

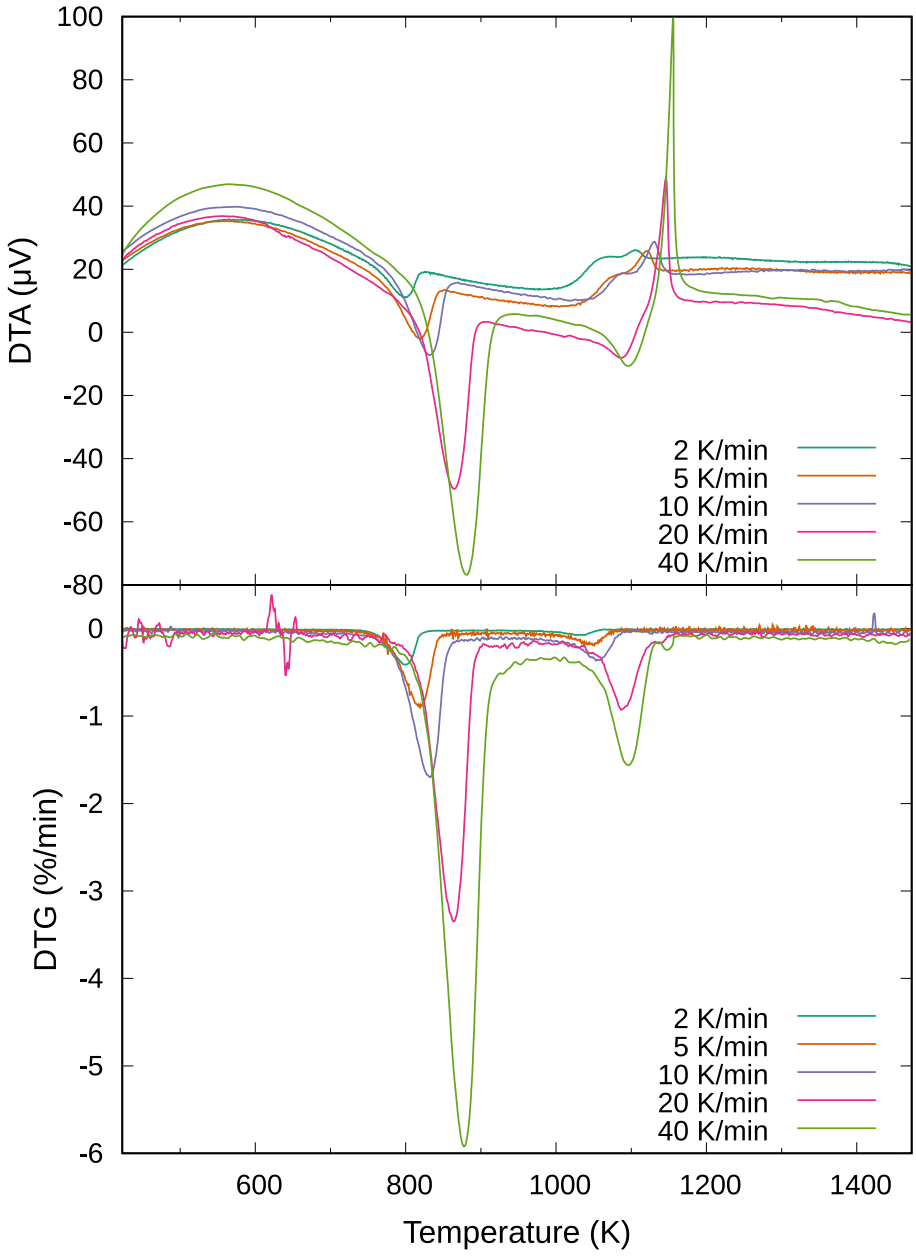

Figure 2.6: DTG and DTA results of dehydroxylation of chlorite CCa-2.

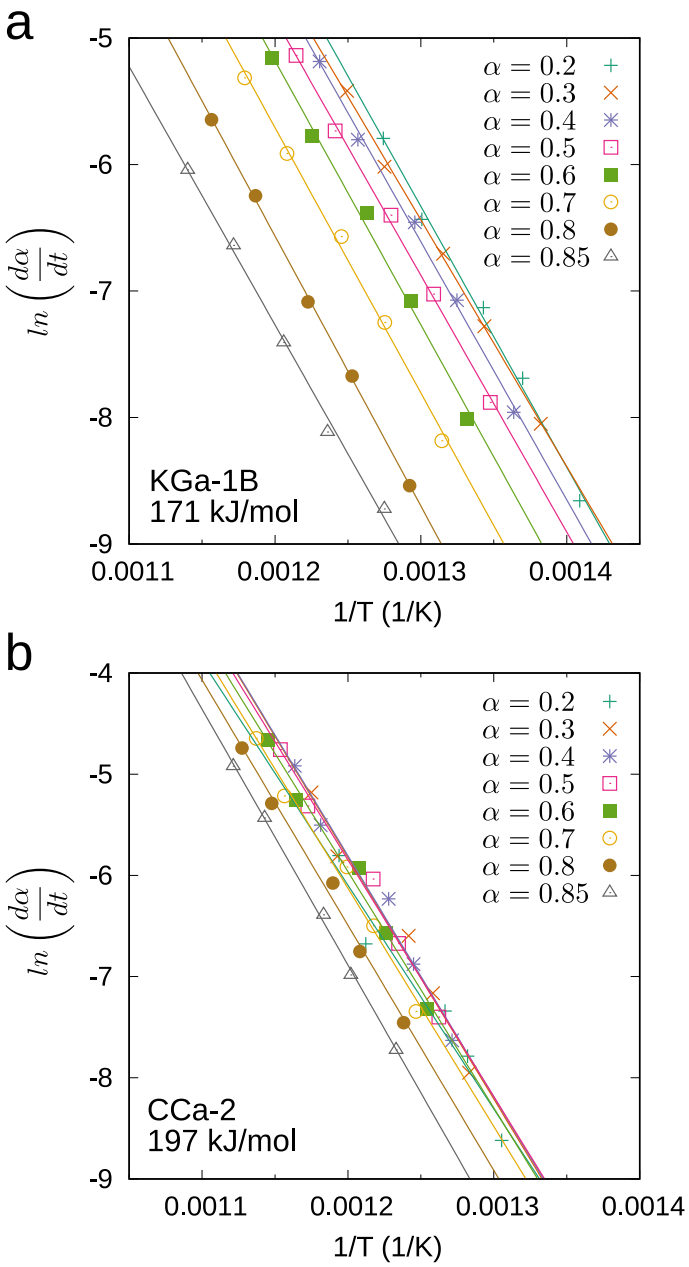

Figure 2.7: Friedman plot for the dehydroxylation of (a) kaolinite KGa-1B and (b) a brucite layer in chlorite CCa-2. Also shown are the activation energies for each reaction determined from these plots.

Table 2.4: Integral expressions for various solid-state kinetic models and determination of the most probable reaction mechanisms (in Bold).

Reaction mechanism	$g(\alpha)$	Heating rate ($K\,min^{-1}$)	2	5	10	20	40	Frequency factor (s^{-1})
			Correlation coefficient					
Kaolinite, KGa-1B								
Reaction-order models								
F_0	α		0.927	0.926	0.923	0.935	0.926	4.8×10^8
F_1	$\ln(1-\alpha)$		0.984	0.984	0.983	0.989	0.985	8.1×10^8
$F_{3/2}$	$(1-\alpha)^{-1/2} - 1$		**0.999**	**0.999**	**0.998**	**1.000**	**0.999**	$\mathbf{5.6 \times 10^8}$
F_2	$(1-\alpha)^{-1} - 1$		0.996	0.996	0.996	0.993	0.995	1.6×10^9
F_3	$(1-\alpha)^{-2} - 1$		0.937	0.937	0.937	0.923	0.932	7.5×10^9
Geometrical contraction models								
R_2	$1-(1-\alpha)^{-1/2}$		0.959	0.958	0.956	0.965	0.959	3.1×10^8
R_3	$1-(1-\alpha)^{-1/3}$		0.968	0.967	0.966	0.974	0.968	2.2×10^8
Nucleation models								
A_2	$[-\ln(1-\alpha)]^{1/2}$		0.890	0.889	0.884	0.899	0.889	7.7×10^8
A_3	$[-\ln(1-\alpha)]^{1/3}$		0.832	0.831	0.825	0.842	0.831	7.7×10^8
A_4	$[-\ln(1-\alpha)]^{1/4}$		0.798	0.797	0.790	0.809	0.796	7.7×10^8
P_2	$\alpha^{1/2}$		0.831	0.830	0.824	0.842	0.830	6.0×10^8
P_3	$\alpha^{1/3}$		0.786	0.785	0.778	0.797	0.785	6.5×10^8
P_4	$\alpha^{1/4}$		0.761	0.760	0.752	0.773	0.760	6.8×10^8
Diffusion models								
D_1	α^2		0.991	0.991	0.991	0.993	0.992	3.2×10^8
D_2	$\alpha + (1-\alpha)\ln(1-\alpha)$		0.994	0.994	0.995	0.994	0.995	2.2×10^8
D_3	$[1-(1-\alpha)^{1/3}]^2$		0.988	0.989	0.989	0.984	0.988	7.1×10^7
D_4	$1-2\alpha/3-(1-\alpha)^{2/3}$		0.993	0.994	0.994	0.992	0.994	5.5×10^7
Chlorite, CCa-2								
Reaction-order models								
F_0	α		0.997	0.992	0.989	0.997	0.995	7.2×10^9
F_1	$\ln(1-\alpha)$		0.987	0.994	0.995	0.987	0.991	1.1×10^{10}
$F_{3/2}$	$(1-\alpha)^{-1/2} - 1$		0.956	0.969	0.972	0.955	0.963	7.5×10^9
F_2	$(1-\alpha)^{-1} - 1$		0.902	0.923	0.926	0.901	0.912	2.1×10^{10}
F_3	$(1-\alpha)^{-2} - 1$		0.748	0.776	0.778	0.743	0.758	8.9×10^{10}
Geometrical contraction models								
R_2	$1-(1-\alpha)^{-1/2}$		**0.999**	**1.000**	**0.999**	**0.999**	**1.000**	$\mathbf{4.5 \times 10^9}$
R_3	$1-(1-\alpha)^{-1/3}$		0.997	0.999	0.999	0.997	0.999	3.2×10^9
Nucleation models								
A_2	$[-\ln(1-\alpha)]^{1/2}$		0.977	0.965	0.959	0.979	0.971	1.2×10^{10}
A_3	$[-\ln(1-\alpha)]^{1/3}$		0.941	0.922	0.913	0.943	0.928	1.2×10^{10}
A_4	$[-\ln(1-\alpha)]^{1/4}$		0.916	0.894	0.884	0.918	0.900	1.3×10^{10}
P_2	$\alpha^{1/2}$		0.945	0.927	0.918	0.947	0.934	9.7×10^9
P_3	$\alpha^{1/3}$		0.911	0.888	0.878	0.913	0.895	1.1×10^{10}
P_4	$\alpha^{1/4}$		0.890	0.866	0.855	0.893	0.872	1.1×10^{10}
Diffusion models								
D_1	α^2		0.948	0.964	0.968	0.949	0.956	4.3×10^9
D_2	$\alpha + (1-\alpha)\ln(1-\alpha)$		0.915	0.936	0.941	0.916	0.926	2.9×10^9
D_3	$[1-(1-\alpha)^{1/3}]^2$		0.867	0.892	0.897	0.868	0.880	9.1×10^8
D_4	$1-2\alpha/3-(1-\alpha)^{2/3}$		0.900	0.922	0.928	0.901	0.912	7.2×10^8

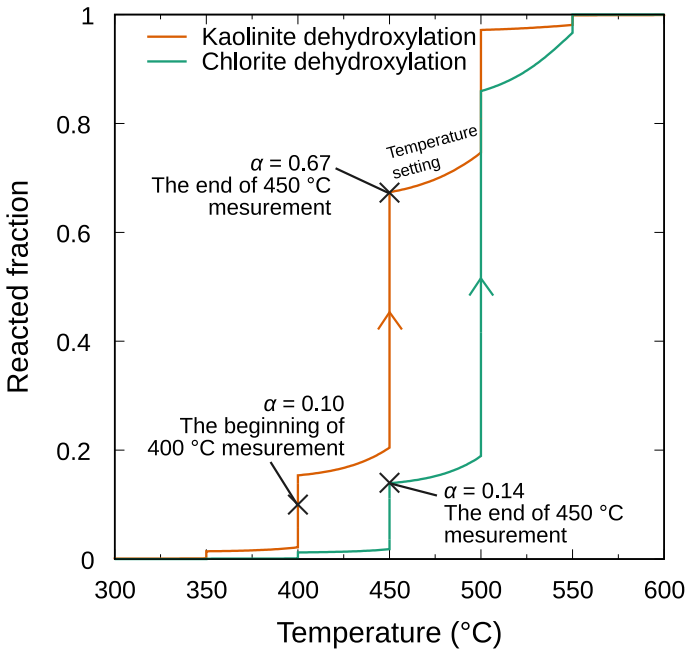

Figure 2.8: Calculated reacted fraction of kaolinite and chlorite dehydroxylation during high-temperature XRD measurements.

have determined correspond to this process.

The kinetic calculations based on these parameters demonstrate that during the XRD experiment a decrease in the normalized K002/C004 value from 1.0 to ~0.6 (Figure 2.3b) coincides with progress of the kaolinite dehydroxylation, from 0.10 to 0.67 reacted portion (Figure 2.8), because the K002 peak intensity should start to decrease between 400 °C and 450 °C during high-temperature XRD experiments. This finding indicates that the normalized K002/C004 value for the Shirako Fault gouge relative to the host rocks (0.74 ± 0.09; Table 2.1) is achieved at a certain moment during this time interval (Figure 2.8), implying that the reacted fractions of 0.10 and 0.67 for kaolinite dehydroxylation are lower and upper bounds of the reaction state, respectively.

We note that the chemical composition of chlorite can affect the dehydroxylation process. For example, the DTA analysis of Smykatz-Kloss (1974) showed that Fe-bearing chlorite ripidolite (from Chaffee Co., USA) decomposes at 581 °C–650 °C, which is higher than the temperature for pure Fe-chlorite

(chamosite; 523 °C) or dioctahedral Al-chlorite (498 °C). Földvári (2011) also examined the thermal behavior of various types of chlorite, and showed that the temperature ranges for the dehydroxylation of the 2:1 layers of Mg-Fe-chlorite (clinochlore), ripidolite, Fe-chlorite (chamosite), and Al-chlorite (sudoite and cookeite) are 835 °C–865 °C, 770 °C–790 °C, 520 °C–580 °C, and 500 °C–530 °C, respectively. However, pure Fe-chlorite and dioctahedral Al-chlorite are rare in the arc–trenchderived rocks of Japan, except Fe-chlorite from veins in hydrothermal ore deposits and Al-chlorite from kuroko-type and pyrophyllite deposits (Shirozu, 1969, 1978a, 1978b), suggesting that chlorite in the subduction settings (which is probably clinochlore–ripidolite) is stable at the temperatures it would have experienced in this system. Thus, the temperature range estimated above is reasonable for the Shirako Fault gouge.

The mechanical effects also appear to have an influence on clay mineral reactions (e.g. Franco et al., 2003; Frost et al., 2001; Vrolijk & van der Pluijm, 1999). The mechanical breakdown, increased surface area of the gouge, and finer grain size in the fault core due to comminution could accelerate the reaction relative to what was measured in the XRD experiments. Vrolijk and van der Pluijm (1999) suggested that faulting helped overcome a kinetic barrier in the smectite-illite reaction. It is inferred that faulting could have also accelerated dehydroxylation reaction of clay minerals. This uncertain factor requires further experimental studies of the kinetic parameters applicable to a short-duration thermal event in a dynamic slip zone environment. On the other hand, fluid infiltrations may also have played an important role on temperature condition along the fault. If warm fluids flowed into the fault during and/or after faulting, the peak temperatures from the above arguments may be overestimated. Further geochemical studies enable us to evaluate fluid–rock interaction at high temperatures within the fault gouge.

2.5 Conclusions

We have investigated the dehydroxylation of kaolinite and chlorite, which are typical components of clay-bearing fault gouges in subduction zones. To provide

quantitative constraints on fault slip behavior, we performed high-temperature XRD experiments and thermogravimetric analyses on these clay minerals. These results allow definition of a relationship between reacted fraction and temperature. Thermal models of frictional heating and their correlation to the experiments demonstrate that dehydroxylation of kaolinite and chlorite can be a new proxy to constrain parameters of earthquake slip event. Further experimental investigations should also address whether mechanical and/or fluid composition can affect dehydroxylation reactions in natural fault zones.

Chapter 3

Application of clay dehydroxylation kinetics to natural fault rock samples: Examples from the megasplay fault in the Nankai Trough and an imbricate thrust in an accretionary prism

3.1 Introduction

Shallow parts of plate subducting margin have a significant role in tsunamigenic earthquake. During the 2011 Tohoku-Oki earthquake (moment magnitude M_w 9.0), the coseismic displacement of ~50–80 m on the megathrust had reached the Japan Trench axis (Fujiwara et al., 2011; Ito et al., 2011), resulted in destructive tsunami. The megasplay fault of the Nankai Trough likely slipped during the 1944 Tonankai

earthquake and generated a tsunami (e.g. G. F. Moore et al., 2007; Park et al., 2002). Core samples of the megasplay fault in the Nankai Trough were recovered during the Integrated Ocean Drilling Program (IODP) Nankai Trough Seismogenic Zone Experiment (NanTroSEIZE) Expedition 316 (Expedition 316 Scientists, 2009; Figure 3.1). Heat signals possibly associated with past earthquake events have been found from the slip zone samples (Fulton & Harris, 2012; Hamada et al., 2015; Hirono et al., 2009, 2014; Sakaguchi et al., 2011; Yamaguchi et al., 2011).

Dehydroxylation is a process common to hydrous clay minerals at elevated temperatures. Several works documented the progression of dehydroxylation reaction within the fault zone possibly triggered by frictional heating (Hirono et al., 2008; Kameda et al., 2013; Kuo et al., 2009, 2011). Kuo et al. (2011) conducted heating experiment of the Taiwan Chelungpu Fault samples and observed that XRD patterns were successively changed with the progress of dehydroxylation reaction. Comparison between the gouge samples and those of heat-treated samples indicate that the experienced temperature of the fault is from 900 °C to 1100 °C. However, this is likely an overestimation since the heating rate adopted in the experiment (150 °C min^{-1}) is much slower than the frictional heating in natural fault zones. In this respect, it is more robust if reaction kinetics is available for such thermal analysis.

In this chapter, I first examined dehydroxylation reactions of the slip zone samples along the megasplay fault in the Nankai Trough and the Shirako Fault. Then, the slip behaviors of these faults are discussed based on the reaction kinetics described in the previous chapter.

3.2 Geological settings

3.2.1 The Shirako Fault in the Miura-Boso accretionary prism

The Shirako Fault is exposed as a member of imbricate thrust system of the Miura-Boso accretionary prism, on the Boso peninsula of central Japan (Kameda

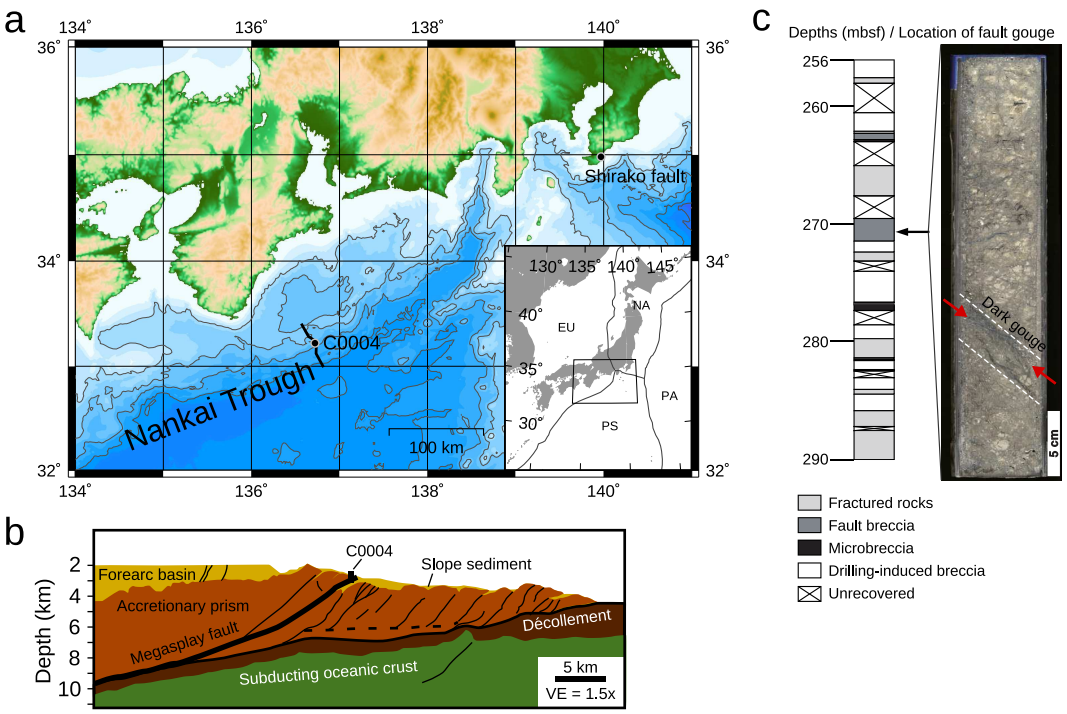

Figure 3.1: (a) Location of the IODP NanTroSEIZE drilling site C0004. The solid line shows the seismic profile line from G. F. Moore et al. (2009). EU, Eurasian plate; NA, North American plate; PS, Philippine Sea plate. (b) Structural interpretation of the megasplay fault zone based on a seismic profile along the NanTroSEIZE drilling transect (after G. F. Moore et al., 2007, 2009; Hamada et al., 2015). (c) Drill hole log and photograph of the core sample (after Expedition 316 Scientists, 2009; Yamaguchi et al., 2011). White dotted lines show the location of a slip zone.

et al., 2013; Figures 3.1a, 3.2a, 3.2b). The host sedimentary sequence of the thrust system (Nishizaki formation) was deposited on the Izu-arc along the Sagami trough (Hanamura & Ogawa, 1993; Lee & Ogawa, 1998; Soh et al., 1989, 1991; Yamamoto & Kawakami, 2005) during 9.9–6.8 Ma (based on radiolarian biostratigraphy; Kawakami, 2001; Yamamoto & Kawakami, 2005). A maximum paleotemperature of ~50 °C and a maximum burial depth of the Nishizaki formation of 1000 m have been estimated based on vitrinite reflectance data (Yamamoto et al., 2005, 2017). The Nishizaki formation sediments also preserve a high porosity (35–50%), which is consistent with maximum burial depth of 1000 m (Yamamoto, 2006; Yamamoto et al., 2005). From detailed structural analyses, Yamamoto et al. (2005) suggest that the thrust system corresponds to an ancient branching fault system of the Miura-Boso accretionary prism.

The Shirako Fault strikes NE to SW, dips ~70° to northward, and is characterized by a black gouge from a few millimeters to centimeters thick (Figures 3.2b–3.2d; Kameda et al., 2013). Under the optical microscope, the black gouge layer has preferred mineral orientation (Kameda et al., 2013), which is very similar to the comparative fault in the Miura peninsula (the Sengen fault; Yamamoto et al., 2005). As mentioned above, the Shirako Fault gouge shows localized claymineral anomaly relative to the host rocks: higher illite fraction in illite-smectite (I-S) mixed layer and lower XRD peak intensity of kaolinite relative to chlorite (Kameda et al., 2013). Based on the above XRD analyses, kaolinite 002 / chlorite 004 peak intensity value ranges 0.45 ± 0.06 in the fault gouge samples, while it ranges 0.60 ± 0.12 in the host siltstone samples (Figure 2.1 and Table 2.1).

3.2.2 The Megasplay fault in the Nankai Trough

The Nankai trough is a subduction margin where the Philippine Sea plate is subducting beneath the Eurasian plate at a rate of ~40 mm/year (Seno et al., 1993). Along the subduction boundary, large earthquakes and accompanying tsunamis repeatedly occurred (e.g. Ando, 1975). To investigate the generation mechanism of the Nankai Trough earthquakes, the International Ocean Drilling Program (IODP)

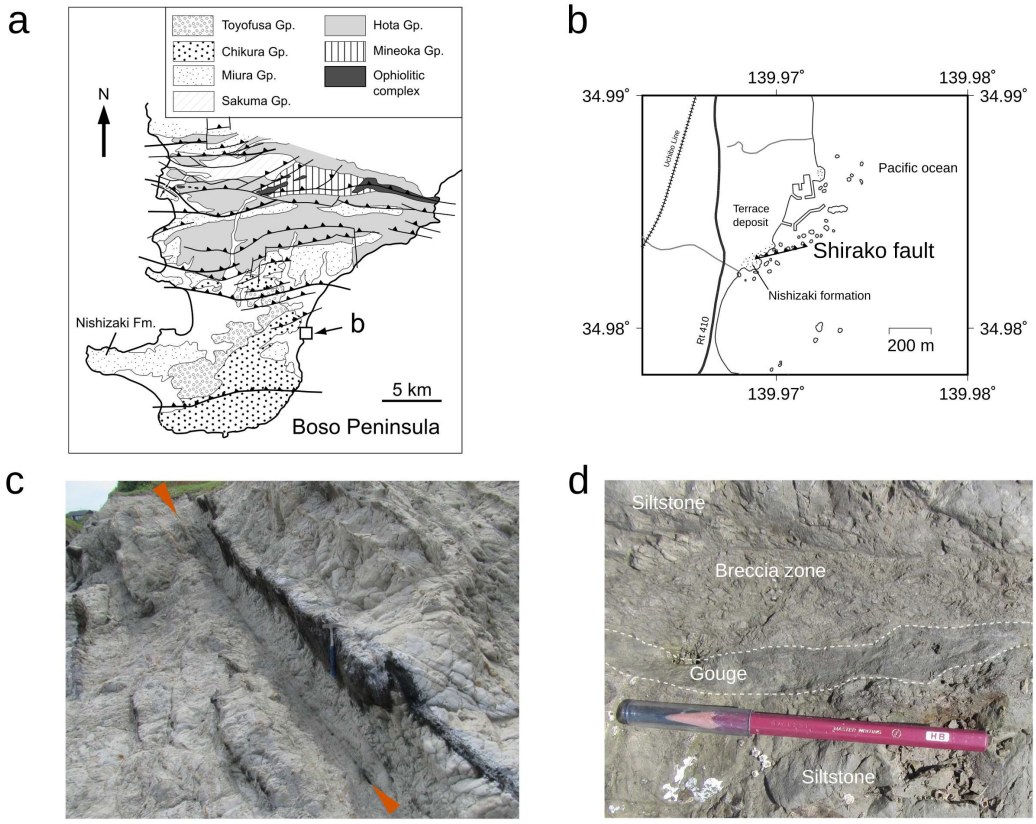

Figure 3.2: (a) Geological map of the Boso peninsula (modified after Yamamoto et al., 2005). (b) Location map of the area around the Shirako Fault after Kameda et al. (2013). (c) Outcrop of the Shirako Fault. Solid arrows show a slip zone of the fault. (d) Occurrence of the Shirako Fault gouge. The ~3-cm-thick black gouge layer is observed along the fault.

Nankai Trough Seismogenic Zone Experiments (NanTroSEIZE), was started in 2007, and have drilled deep holes along the transect off the Kii peninsula and recovered core samples from the megasplay fault and the frontal décollement (Figure 3.1; G. F. Moore et al., 2009). At this location, coseismic rupture propagated along the Nankai trough during the 1944 Tonankai earthquake (Baba & Cummins, 2005; Ichinose et al., 2003). Many authors discussed that large cosesmic slip propagated along the megasplay fault during past earthquakes (Baba & Cummins, 2005; Baba et al., 2006; G. F. Moore et al., 2007; Park et al., 2002).

Recently, Sakaguchi et al. (2011) reported vitrinite reflectance anomaly along the megasplay fault and along the frontal décollement and concluded that seismic ruptures propagated near the seafloor on these faults. Fulton and Harris (2012) and Hamada et al. (2015) reanalyzed the data from Sakaguchi et al. (2011), and Hamada et al. (2015) reported frictional heating of ~330 °C along the megasplay fault. Yamaguchi et al. (2011) documented the local progression of the S–I reaction in a fault gouge, relative to host sediments, of the megasplay fault.

3.3 Materials and methods

3.3.1 Samples

Fault gouge material of the megasplay fault was recovered from 271 m below the seafloor (mbsf) at Site C0004 during IODP Expedition 316 (December 2007–February 2008; Kimura et al., 2008) (Figure 3.1). The clay-fraction mineralogy of the black gouge that developed along the megasplay fault of the Nankai Trough was examined by Yamaguchi et al. (2011). During the present study, we quantified the clay mineralogy of the same retrieved gouge material as well as host sediments recovered from the drill hole.

To prepare the gouge samples for analysis, they were first gently crushed and dispersed ultrasonically in distilled water. The clay fraction (<2 μm spherical equivalent) of each sample was then separated by centrifugation and washed three times in 1 M $CaCl_2$ to prepare Ca-saturated specimens. Suspensions

of Ca-saturated specimens were dropped onto glass slides to prepare oriented mounts by air-drying in an oven at 60 °C. These mounts were saturated with ethylene-glycol vapor at 60 °C overnight (herein referred to as the "EG" state).

3.3.2 X-ray diffraction analysis

XRD profiles for oriented mounts of clay fraction were obtained from 24° to 26° 2θ using a Rigaku SmartLab with monochromatized Cu$K\alpha$ radiation at 45 kV and 200 mA, with 1/4° divergence and anti-scattering slits, and a 0.30-mm receiving slit in continuous scan mode at a rate of 0.1° 2θ per minute. We used Macdiff (version 4.2.6) software developed by Petschick (2010) to calculate baselines, decompose peaks based on Pearson-type VII function, and measures the integrated peak intensity of individual peaks. Obtained peak profile decomposed into K002 and C004 peaks and each integrated peak intensity using this software. Full width at half maximum (FWHM) of K001 + C002 overlapped peak were also obtained from EG XRD patterns for these core samples from the data in chapter 4.3.

3.3.3 Numerical analysis of frictional heating

To evaluate the temperatures experienced by a fault gouge during an earthquake slip event, we combined thermal modeling of frictional heating and kinetic simulations of kaolinite and chlorite dehydroxylation reactions. Anomalous temperature, $U(x, t)$, at a shear plane-perpendicular distance, x, from the center of the slip zone can be expressed as

$$U(x,t) = \frac{\tau}{\rho C_p}\frac{vt}{a}\left[1 - 2\mathrm{i}^2\mathrm{erfc}\left(\frac{a-x}{\sqrt{4\kappa t}}\right) - 2\mathrm{i}^2\mathrm{erfc}\left(\frac{a+x}{\sqrt{4\kappa t}}\right)\right] \quad (t \le t^*, x \le a) \quad (3.1)$$

$$U(x,t) = \frac{\tau}{\rho C_p}\frac{v}{a}\left\{t\left[1 - 2\mathrm{i}^2\mathrm{erfc}\left(\frac{a-x}{\sqrt{4\kappa t}}\right) - 2\mathrm{i}^2\mathrm{erfc}\left(\frac{a+x}{\sqrt{4\kappa t}}\right)\right]\right.$$
$$\left. - (t-t^*)\left[1 - 2\mathrm{i}^2\mathrm{erfc}\left(\frac{a-x}{\sqrt{4\kappa\,(t-t^*)}}\right) - 2\mathrm{i}^2\mathrm{erfc}\left(\frac{a+x}{\sqrt{4\kappa\,(t-t^*)}}\right)\right]\right\} \quad (t > t^*, x \le a) \quad (3.2)$$

where t is the time, t^* is the duration of the slip event, τ is the shear stress, $2v$ is the slip velocity, ρ is the density, C_p is the specific heat capacity, $2a$ is the thickness of the heat source (slip zone), and κ is the thermal diffusivity, respectively (Carslaw & Jaeger, 1959; Lachenbruch, 1980, 1986). The $\mathrm{i}^2\mathrm{erfc}(\beta)$ is the second integral of the complementary error function of β and can be written as follows (e.g. Carslaw & Jaeger, 1959):

$$\mathrm{i}^2\mathrm{erfc}(\beta) = \frac{1}{4}\left[(1+2\beta^2)\mathrm{erfc}(\beta) - \frac{2}{\sqrt{\pi}}\beta\exp(-\beta^2)\right]. \tag{3.3}$$

We simulated temperature of the center of the slip zone using equations (3.1)–(3.3). The temperature rise (equations (3.1) and (3.2)) shows a direct trade-off between shear stress and slip amount (heat deposition at the fault scales linearly with the product of the two) during faulting. The temperature rise is inversely proportional to thickness and for long duration events are mediated by the diffusion of heat away from the fault during slip.

For our numerical analysis for the Shirako Fault, we adopted the "base slip condition" equal to the analysis of Kameda et al. (2013): heat source thickness of 3 cm, initial temperature of 52 °C (325 K) derived from vitrinite reflectance data (Yamamoto et al., 2005), and slip rate of 1 m s^{-1}. The shear stress was calculated by assuming a hydrostatic overburden pressure (σ_v) corresponding to a burial depth of 1.5 km, a slip plane dipping at 10°, and a dynamic friction coefficient, μ, of 0.6. The slip duration was varied to control the peak temperature of slip plane and the calculation was continued until the temperature cooled to 150 °C (423 K). The parameters used for the calculations for the Shirako Fault are summarized in Table 3.1. We tested variations of the free parameters, μ (0.6, 0.3, and 0.1), slip rate (1, 0.1, and 0.01 m s^{-1}), and heat source thickness (3, 1, 0.3, and 0.1 cm; we consider that 3 cm is an upper bound because it is equivalent to the observed gouge thickness), with the base slip condition. We also tested a case with a repetition of 10 and 100 identical events. Each event was modeled with the base slip condition.

For the Nankai megasplay fault, we obtained thermophysical property of the sediment from Kinoshita et al. (2009). Initial temperature of 20 °C, shear stress of

Table 3.1: Parameters used for numerical analyses for the Shirako Fault with the base slip condition.

Parameters	Symbol	Value	References
Initial temperature	T_0	325 K	Yamamoto et al. (2005)
Bulk density	ρ	2105 kg m^{-3}	Kameda et al. (2013)
Specific heat capacity	C_p	1.61 J kg^{-1} K^{-1}	Hamada et al. (2011) and Kameda et al (2013)
Thermal diffusivity	κ	2.7×10^{-7} m^2 s^{-1}	Hamada et al. (2011) and Kameda et al (2013)
Shear stress	τ	7.54 MPa	Kameda et al. (2013)
Heat source thickness	$2a$	0.03 m	Kameda et al. (2013)
Slip velocity	$2v$	1 m s^{-1}	Kameda et al. (2013)

Table 3.2: Parameters used for numerical calculation for the Nankai megasplay fault with the base slip condition.

Parameters	Symbol	Value	References
Initial temperature	T_0	293 K	Hamada et al. (2015)
Bulk density	ρ	1800 kg m^{-3}	Kinoshita et al. (2009)
Specific heat capacity	C_p	1.8 J kg^{-1} K^{-1}	Kinoshita et al. (2009)
Thermal diffusivity	κ	5.0×10^{-7} m^2 s^{-1}	Kinoshita et al. (2009)
Shear stress	τ	1.83 MPa	Hamada et al. (2015)
Heat source thickness	$2a$	0.01 m	Hamada et al. (2015)
Slip velocity	$2v$	0.01 m s^{-1}	Hamada et al. (2015)

1.83 MPa, heat source thickness of 0.01 m, and slip velocity of 0.01 m s^{-1} are taken from Hamada et al. (2015). Friction coefficient of 0.4 is obtained from Ikari et al. (2009). Parameters used for numerical calculation with the base slip condition are summarized in Table 3.2. We tested variations of slip velocity (1, 0.1, 0.01, and 0.001 m s^{-1}), friction coefficient (0.4, 0.2, and 0.1), and width of the heat source (1, 0.3, and 0.1 cm). We also calculated with a repetition of 10 and 100 identical slip events.

3.4 Results

3.4.1 The Shirako Fault in the Miura-Boso accretionary prism

Reaction modeling of base slip condition associated with potential frictional heating events along the Shirako Fault demonstrates a dependence on peak

temperature during faulting (Figure 3.3a). Comparison of the fractional progress of dehydroxylation reactions for kaolinite and chlorite to the peak temperatures calculated in the thermal models reveals that kaolinite dehydroxylation occur in lower temperature than for chlorite dehydroxylation in the fault gouge. Figures 3.3b–d show the results with a single frictional heating event, and Figure 3.3e shows the case with a repetition of 10 and 100 identical events.

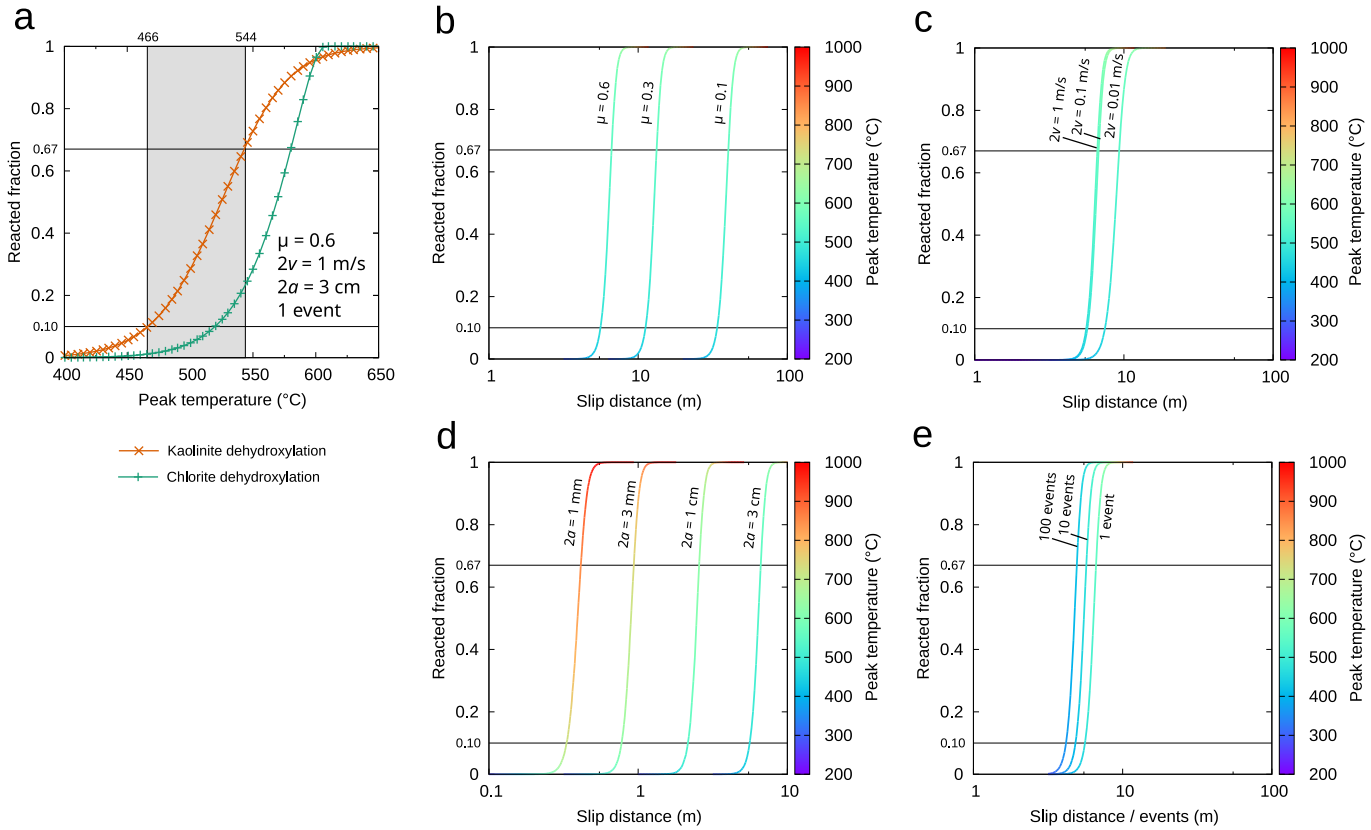

Figure 3.3: (a) Reacted fraction of kaolinite and chlorite dehydroxylation plotted versus the calculated peak temperature during the modeled coseismic slip with each combination of slip parameters. The results for the base slip condition, $2v$ = 1 m s^{-1}, μ = 0.6, $2a$ = 3 cm. The shaded area indicates the possible slip conditions which correspond to kaolinite reacted fraction of 0.10–0.67. (b – e) Reacted fraction of kaolinite dehydroxylation versus slip distance. Each panel shows variation of (b) friction coefficient, (c) slip velocity, (d) fault thicknesses, and (e) number of multiple events. The line color indicates the peak temperature for simulated slip events.

3.4.2 The Megasplay fault in the Nankai Trough

Result of XRD analysis for the fault gouge and host sediment samples are shown in Figure 3.4. 7 Å reflections of K002 and C004 are observed in the fault and host samples. Peak decomposition analysis results are summarized in Table 3.3 and Figure 3.5. For the fault gouge sample, observed K002 / C004 peak intensity ratio (0.429) is particularly smaller than host samples (0.684) (Table 3.3). As a consequence, host-normalized K002 / C004 value for the fault gouge sample is 0.667. This is consistent with the results for the Shirako Fault in the the Miura-Boso accretionary prism (Kameda et al., 2013; Table 2.1; Figure 2.1). FWHM of K001 + C002 for the fault gouge sample (0.34) is also relatively smaller than host (0.39 ± 0.03) (Table 3.4). This result is consistent with the results for the Shirako Fault (Kameda et al., 2013). Figure 3.6 shows the results of numerical calculation. Reacted fraction for kaolinite dehydroxylation versus slip velocity and peak transient temperature are plotted on the panels.

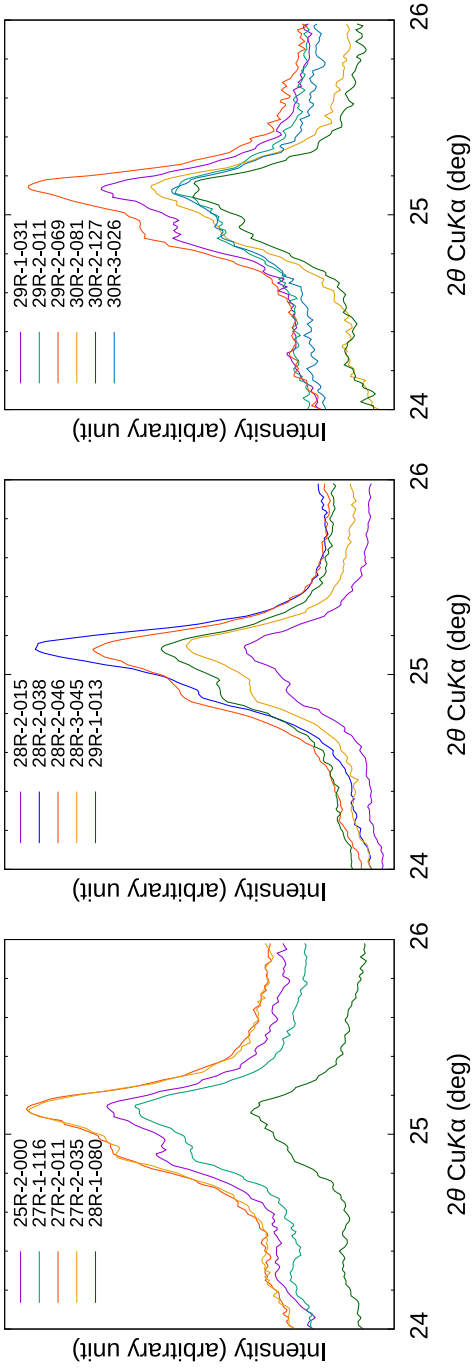

Figure 3.4: X-ray diffraction patterns for the clay fraction (<2 µm) of Site C0004 sediments.

Table 3.3: Results of peak analysis for XRD profiles for K002 and C004. Data of the fault gouge are marked by bold.

		K002			C004			K002/C004	Normalized
Sample name	Depth (mbsf)	Position (deg)	Area (cps)	FWHM (deg)	Position (deg)	Area (cps)	FWHM (deg)		K002/C004
25R-2-000	257.41	24.87	15234	0.33	25.13	21410	0.30	0.711	1.11
27R-1-116	266.16	24.89	12199	0.30	25.13	18256	0.27	0.668	1.04
27R-2-011	266.52	24.89	17230	0.30	25.13	27411	0.27	0.629	0.979
27R-2-035	266.76	24.89	16186	0.30	25.13	26921	0.27	0.601	0.937
28R-1-080	270.30	24.91	7775	0.32	25.12	13019	0.29	0.597	0.930
28R-2-015	271.06	24.89	14630	0.31	25.14	23289	0.28	0.628	0.977
28R-2-038	**271.29**	**24.89**	**20521**	**0.28**	**25.14**	**47883**	**0.25**	**0.429**	**0.667**
28R-2-046	271.37	24.88	25859	0.30	25.13	42464	0.27	0.609	0.949
28R-3-045	272.77	24.89	18370	0.30	25.15	28313	0.26	0.649	1.01
29R-1-013	274.13	24.88	19111	0.30	25.13	30347	0.28	0.630	0.981
29R-1-031	274.31	24.89	10496	0.30	25.13	16797	0.27	0.625	0.974
29R-2-011	275.51	24.88	20109	0.32	25.12	29918	0.28	0.672	1.05
29R-2-069	276.09	24.89	12268	0.29	25.14	21824	0.26	0.562	0.876
30R-2-081	280.72	24.89	10619	0.34	25.14	18139	0.31	0.585	0.912
30R-2-127	281.18	24.88	20476	0.36	25.13	26347	0.31	0.777	1.21
30R-3-026	281.58	24.89	8116	0.30	25.13	11867	0.26	0.684	1.07
Average of host sediment				0.31			0.28		
2σ				0.04			0.03		

Table 3.4: Results of peak analysis for XRD profiles for K001 + C002. Data of the fault gouge are marked by bold.

Sample name	Depth (mbsf)	Position (deg)	Area (cps)	FWHM (deg)
25R-2-000	257.41	12.44	12435	0.42
27R-1-116	266.16	12.44	16752	0.41
27R-2-011	266.52	12.44	18733	0.39
27R-2-035	266.76	12.44	20660	0.38
28R-1-080	270.30	12.42	8921	0.40
28R-2-015	271.06	12.46	15982	0.41
28R-2-038	**271.29**	**12.42**	**33324**	**0.34**
28R-2-046	271.37	12.44	31045	0.39
28R-3-045	272.77	12.46	20223	0.39
29R-1-013	274.13	12.42	24890	0.40
29R-1-031	274.31	12.46	13859	0.37
29R-2-011	275.51	12.44	13283	0.40
29R-2-069	276.09	12.44	15815	0.36
30R-2-081	280.72	12.46	8064	0.39
30R-2-127	281.18	12.44	11029	0.40
30R-3-026	281.58	12.46	11150	0.41
Average of host sediment				0.39
2σ				0.03

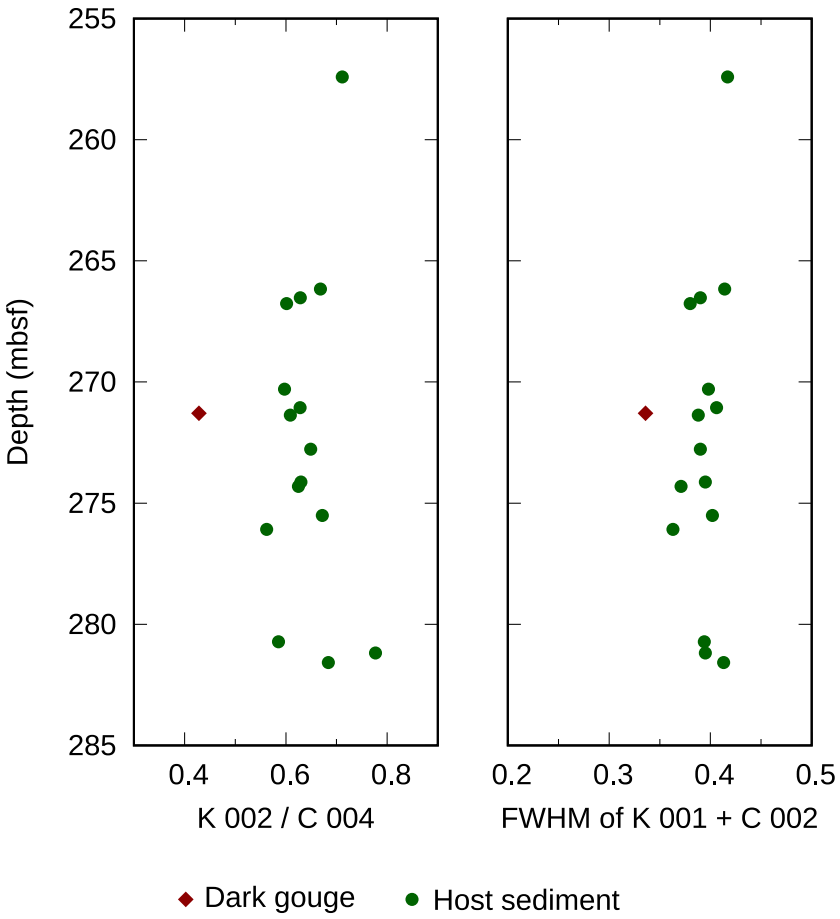

Figure 3.5: Depth (mbsf) versus integrated peak area of kaolinite 002 / chlorite 004 and FWHM of kaolinite 001 + chlorite 002 peak.

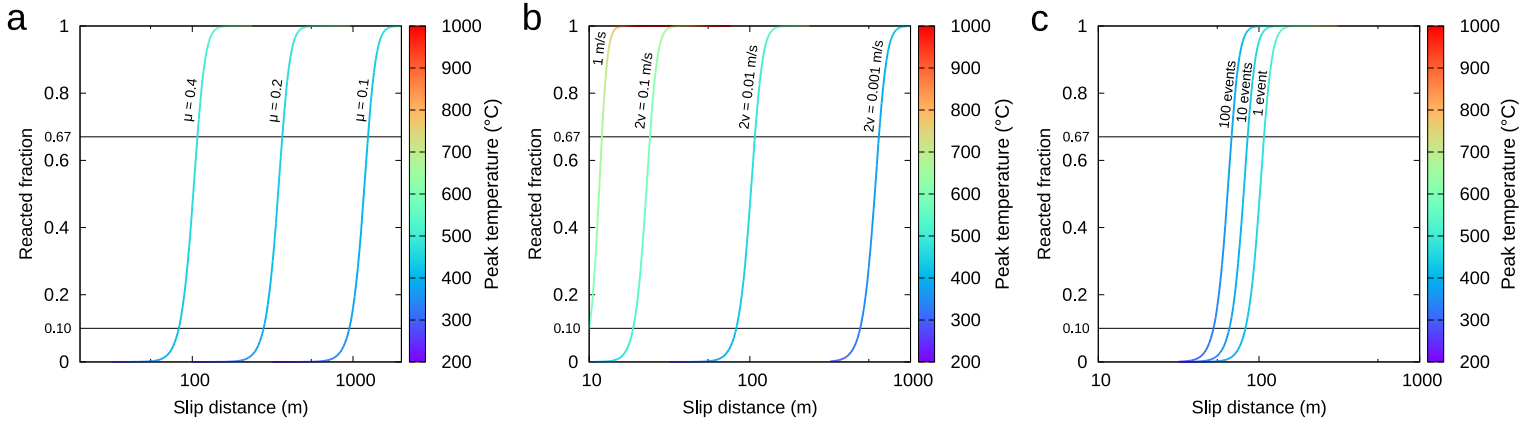

Figure 3.6: Reacted fraction of kaolinite dehydroxylation versus slip distance. Each panel shows variation of (a) friction coefficient, (b) slip velocity, (c) number of multiple events. The line color indicates the peak temperature for simulated slip events.

3.5 Discussions

3.5.1 The Shirako Fault in the Miura-Boso accretionary prism

In chapter 2, we found that the normalized K002/C004 value for the Shirako Fault gouge relative to the host rocks (0.74 ± 0.09; Table 2.1) is achieved at a certain moment during this time interval (Figure 2.8), implying that the reacted fractions of 0.10 and 0.67 for kaolinite dehydroxylation are lower and upper bounds of the reaction state, respectively. If we assume a single heating event with the base slip condition, our reaction models yield a peak transient temperature of <~460 °C (Figure 3.3a and Table 3.5), implying that both kaolinite and chlorite dehydroxylation will not observe by XRD peak intensity. In this case, the reacted fraction of kaolinite dehydroxylation should remain less than 0.10. On the other hand, nearly complete disappearance of K002 is expected for a slip with a peak temperature greater than ~550 °C, represented by the reacted fraction of >0.67 (Figure 3.3a and Table 3.5). Therefore, the peak temperature and slip displacement for the single slip event can be constrained to be ~460–550 °C and ~5.6 m to ~6.7 m, respectively. It is noted that these temperature bounds are not sensitive to the slip parameters such as the slip velocity and friction coefficient, and any set of these parameters yields the peak temperatures within the range from ~460 °C to ~550 °C (Figures 3.3b, 3.3c, and Table 3.5); however, several parameters have yet to be fully clarified to give more robust temperature constrain. For example, the active slip zone is 3 cm wide in the above calculations, but a thinner slip zone would generate a higher temperature to reproduce the observation (Figure 3.3d and Table 3.5). In the case of 0.1 cm thick of the heat source, the peak temperature can be ~710–850 °C. We also note that the peak temperature decreases to a certain amount if considering repetitive seismic events on this fault (Figure 3.3e and Table 3.5). The peak temperature successively decreases with increase in cumulative number of slips, and in the case of 100 events, the temperature decreases down to ~360–420 °C with the total slip distance of ~420–490 m (Table 3.5). This repeat count may be

the upper bound because the total displacement along the thrust system of the Shirako Fault is 400–500 m (Kameda et al., 2013). Careful field and microtextural observations are necessary to give further insights into the slip behaviors of the fault.

Table 3.5: Slip parameters for the calculation of frictional heating along the Shirako Fault.

				0.10 of reacted fraction for kaolinite dehydroxylation		0.67 of reacted fraction for kaolinite dehydroxylation	
Number of slip event	Width of the heat source (cm)	Slip velocity ($m\,s^{-1}$)	Friction coefficient	Slip distance (m)	Peak temperature (°C)	Slip distance (m)	Peak temperature (°C)
1	3	1	0.6	5.6	460	6.7	550
1	3	1	0.3	11	460	13	550
1	3	1	0.1	34	470	40	550
1	3	0.1	0.6	5.7	470	6.8	550
1	3	0.01	0.6	7.4	460	9.3	530
1	1	1	0.6	2.1	530	2.6	620
1	0.3	1	0.6	0.77	620	0.94	740
1	0.1	1	0.6	0.33	710	0.41	850
10	3	1	0.6	4.8	410	5.7	470
100	3	1	0.6	4.2	360	4.9	420

Note: Slip distance for multiple events shows a distance per events.

3.5.2 The Megasplay fault in the Nankai Trough

Our XRD analysis revealed that kaolinite decomposes selectively within the gouge on the megasplay fault in the Nankai trough (Figure 3.5). If we assume slip velocity of 0.01 m s^{-1}, friction coefficient of 0.4, and width of the heat source of 1 cm (Hamada et al., 2015) with a single heating event, peak transient temperature of ~420–470 °C can explain the selective decomposition of kaolinite (Figure 3.6 and Table 3.6). On the other hand, Hamada et al. (2015) suggested that peak temperature of ~330 °C reproduce an observed vitrinite reflectance anomaly with the slip distance of 56.7 m. Hirono et al. (2009) suggested that the fault gouge has not experienced >400 °C, based on magnetic hysteresis analysis of Site C0004 sediments including the fault gouge samples. This base slip condition may not be likely for the fault gouge and 400 °C may be upper bound temperature during slip.

We tested variations of the free parameters and repetition of heating events. Friction coefficient is varied from 0.4 to 0.1 with slip velocity of 0.01 m s^{-1} and a single heating event (Figure 3.6a and Table 3.6). The peak temperature ranges below 400 °C in the cases of friction coefficient of 0.2 and 0.1. However, because friction coefficient of ~0.4 is estimated by friction experiments of Site C0004 core samples (Ikari et al., 2009; Tsutsumi et al., 2011), other factors, such as slip velocity or repeated slip events, may lower peak temperature of the fault gouge. We tested various slip velocity (1, 0.1, 0.01, and 0.001 m s^{-1}) with friction coefficient of 0.4 and a single heating event (Figure 3.6b and Table 3.6). Among these cases, 0.001 m s^{-1} event is consistent with the temperature condition of Hirono et al. (2009). Variations of width of the heat source show small effect to peak transient temperature (Table 3.6). Effect of cumulative slip events is also tested with slip velocity of 0.01 m s^{-1} and friction coefficient of 0.4 (Figure 3.6c and Table 3.6). If we adopt 10 and 100 repeated events, peak transient temperature ranges below 400 °C. In the case of 100 repeated events, total slip distance ranges from ~5200 m to ~6700 m. This slip distance may be unrealistic because no paleotemperature anomaly between foot wall and hanging wall of the megasplay fault (Sakaguchi et al., 2011). A repetition of ~10 events may occur along the fault gouge with the slip

distance of 660–850 m. On the other hand, Hirono et al. (2014) reported that the fault gouge has not experienced ≥250 °C based on trace-elements geochemistry. The authors found no fluid-rock interaction in ≥250 °C because anomaly in Li, Cs, Sr, and Rb did not observed in the fault gouge. However, our simulation suggest that the fault gouge experienced over 330 °C. This may indicate that lower fluid-rock ratio in the slip zone when the slip events occur (Hamada et al., 2015).

Our simulation shows that frictional heating of ~330–400 °C can explain selective decomposition of kaolinite with repeated slip events and/or slip velocity of ~0.001 m s^{-1}. Our result also suggests repeated slip propagations to shallow part along megasplay fault. The temperature range of frictional heating is consistent with the result based on vitrinite reflectance anomaly (Hamada et al., 2015), but slightly higher than the result based on trace-elements geochemistry (Hirono et al., 2014). The difference suggests that mechanochemical effect might influence the reaction within the fault gouge during slip. Further experimental investigations are needed to estimate mechanochemical effects on clay minerals dehydroxylation reaction.

Table 3.6: Slip parameters for the calculation of frictional heating along the Shirako Fault.

				0.10 of reacted fraction for kaolinite dehydroxylation		0.67 of reacted fraction for kaolinite dehydroxylation	
Number of slip event	Width of the heat source (cm)	Slip velocity ($m\,s^{-1}$)	Friction coefficient	Slip distance (m)	Peak temperature (°C)	Slip distance (m)	Peak temperature (°C)
1	1	1	0.4	10	560	12	660
1	1	0.1	0.4	19	510	24	590
1	1	0.01	0.4	83	420	110	470
1	1	0.001	0.4	490	330	630	380
1	1	0.01	0.2	280	390	360	440
1	1	0.01	0.1	950	360	1240	410
1	0.3	0.01	0.4	83	420	110	470
1	0.1	0.01	0.4	83	420	110	470
10	1	0.01	0.4	66	370	85	420
100	1	0.01	0.4	52	330	67	380

Note: Slip distance for multiple events shows a distance per events.

3.6 Conclusions

We conducted X-ray diffraction analysis and thermal modeling to assess selective breakdown of kaolinite clay mineral within the slip zone on the megasplay fault in the Nankai trough and fossil imbricate thrust in an ancient accretionary prism. The results revealed selective decomposition of kaolinite, relative to chlorite, within the fault gouge along these faults. Our numerical analysis demonstrated that the reaction can be achieved with repeated slip events that are consistent with previous estimation based on vitrinite reflectance and illitization reaction. The result suggests that coseismic slip repeatedly propagations to shallow part along the faults. Further field and microtextural observations, and experimental investigations are needed to clarify uncertain factors, such as cumulative slip effect and mechanochemical effect.

Chapter 4

Lowering of the kinetic barrier of clay-mineral reactions in a seismogenic fault: Example from the Nankai subduction zone

4.1 Introduction

Coseismic slip propagation to the very shallow parts of megathrusts in subduction zones is of particular importance for understanding tsunamigenic earthquakes. Direct measurements of residual temperatures after such earthquakes have revealed the fundamental parameters of megathrusts, including the frictional coefficient and stress state of such faults (e.g. Fulton et al., 2013). Geothermometry has also been used to investigate past earthquake events on ancient or active faults (e.g. O'Hara, 2004; Sakaguchi et al., 2007, 2011). However, it is thought that in addition to thermogenesis, coseismic slip mechanically damages fault rock materials (mechanochemical process), resulting in the modification of chemical reaction kinetics in the fault zone (Hirono et al., 2013). Consequently, available geothermometers in the literature need to be adjusted to be applicable to such a dynamic environment. It has also been suggested that reactions in fault zones

can be promoted by the lowering of kinetic barriers due to faulting-related mechanochemical processes (Vrolijk & van der Pluijm, 1999), but the actual effects of such processes along seismogenic faults are poorly understood.

The smectite-to-illite conversion (S–I) reaction is a common diagenetic reaction in sedimentary basins (e.g. Burst Jr., 1957; Perry & Hower, 1970; Hower et al., 1976). The mechanism for the reaction has been discussed previously (e.g. Altaner & Ylagan, 1997; Lanson et al., 2009; Środoń et al., 2000), with solid-state transformation models (e.g. Bethke & Altaner, 1986; Cuadros & Altaner, 1998; Hower et al., 1976) and dissolution–crystallization models (e.g. Ahn & Peacor, 1986; Boles & Franks, 1979; Inoue, 1987; Nadeau et al., 1985) being widely accepted (Cuadros, 2012). The reaction progresses via intermediate products of mixed-layer illite/smectite (I/S), whose conversion rate generally obeys an Arrhenius-type rate law (Eberl & Hower, 1976; Elliott et al., 1991; Howard & Roy, 1985; Huang et al., 1993; Pytte & Reynolds, 1989; Roberson & Lahann, 1981; Velde & Vasseur, 1992). As smectite is also a typical clay component of crustal faults, application of S–I reaction kinetics should be a valuable tool for investigating the thermal histories of such faults.

A mineralogical analysis by Yamaguchi et al. (2011) documented the local progression of the S–I reaction in a fault gouge, relative to host sediments, of the megasplay fault of the Nankai Trough. Kameda et al. (2013) also found a local progression of the illitization reaction in a slip zone of the Shirako Fault (Miura–Boso accretionary complex) (Figure 3.1a). The geologic setting of the Shirako fault is shallow part of subduction zone megathrust and comparable to that of the megasplay fault of the Nankai Trough. These findings of Kameda et al. (2013) suggest that the reaction progressed by transient heating due to high-velocity seismic slip propagating to very shallow crustal depths (<1.5 km). Based on the rate law of the S–I reaction (Pytte & Reynolds, 1989), the observed reaction may have progressed by repeated slip with maximum temperatures of ~450 °C (Kameda et al., 2013). However, this may be an overestimation if the kinetic barrier was mechanochemically lowered by the coseismic slip (Vrolijk & van der Pluijm, 1999). Many authors have experimentally observed that mechanical effects

lower the temperatures of clay-mineral dehydroxylation reactions (e.g. Aglietti et al., 1986; Pérez-Maqueda et al., 2004; Sánchez-Soto et al., 2000; Sugiyama et al., 1994). Klevtsov et al. (1988) demonstrated that the activation energy of kaolinite dehydroxylation decreased after mechanochemical treatment, and Ptáček et al. (2013) conducted XRD and thermal analysis that revealed the apparent activation energy for the dehydroxylation of ordered kaolinite (~216 kJ mol^{-1}) is markedly higher than that of completely disordered kaolinite (~77 kJ mol^{-1}). Therefore, mechanochemical effects may affect the S–I reaction and lower its apparent activation energy during faulting.

One way to develop the appropriate reaction kinetics is to extract experimentally reasonable parameters from materials that have undergone mechanochemical treatments in the laboratory (Hirono et al., 2013; Kaneki et al., 2018). Another approach is to calibrate the rate law by using natural samples based on well-constrained thermal histories (e.g. Cuadros, 2006; Inoue et al., 1992). The latter is preferable because laboratory experiments of S–I reaction kinetics have often encountered difficulty in assessing the degree of progression of the reaction from the intermediate products (e.g. Cuadros & Linares, 1996). Recently, Hamada et al. (2015) reanalyzed vitrinite reflectance data of organic particles dispersed around the megasplay fault of the Nankai Trough (Sakaguchi et al., 2011) and reproduced a robust thermal history associated with the past seismic slip on this fault. The procedure in that study seems valid, given that only those vitrinite particles outside the slip plane were used for the thermal modeling, thus fully eliminating any mechanochemical effect on the analytical result. In this study, we reexamine the S–I reaction around the slip zone of the Nankai megasplay fault. The reliable thermal history established for this fault allows us to evaluate the mechanochemical effect on the S–I reaction in the seismogenic fault zone.

4.2 Materials and methods

Fault gouge material of the megasplay fault was recovered from 271 m below the seafloor (mbsf) at Site C0004 during IODP Expedition 316 (December 2007–

February 2008; Kimura et al., 2008) (Figure 3.1). Previous qualitative mineralogical analysis using XRD by Yamaguchi et al. (2011) revealed that illitization has occurred in the slip zone of the Nankai megasplay fault. This finding was also supported by high K and Al concentrations in the high-resolution X-ray fluorescence mapping image of the slip zone (Yamaguchi et al., 2011). During the present study, we quantified the clay mineralogy of the retrieved gouge material as well as host sediments recovered from the drill hole.

To prepare the gouge and host sediments samples for analysis, they were first gently crushed and dispersed ultrasonically in distilled water. The clay fraction (<2.0 μm spherical equivalent) of each sample was then separated by centrifugation and washed three times in 1 M $CaCl_2$ to prepare Ca-saturated specimens. Suspensions of Ca-saturated specimens were dropped onto glass slides to prepare oriented mounts by air-drying in an oven at 60 °C. These mounts were saturated with ethylene-glycol vapor at 60 °C overnight (herein referred to as the "EG" state). XRD patterns for oriented mounts were obtained from 2° to 35° 2θ using a MAC Science MX-Labo with monochromatized Cu$K\alpha$ radiation at 40 kV and 30 mA, with 1° divergence and anti-scattering slits, and a 0.15-mm receiving slit in continuous scan mode at a rate of 1° 2θ per minute. The percentage of illite content in I/S (herein termed "$\%I$") was estimated from the saddle/001 peak intensity ratio of EG XRD patterns using the working curve proposed by Inoue et al. (1989). The background was drawn from a spectrum of a glass holder (Inoue et al., 1989). The relative weight proportions of I–S, illite, and kaolinite + chlorite were quantitatively determined by using the weighting factors of Biscaye (1965) and following a similar study undertaken by Guo and Underwood (2012). We used Macdiff (version 4.2.6) software developed by Petschick (2010) to calculate baselines and analyze peak profiles.

There are several models of S–I reaction kinetics with reaction orders from first (e.g. Eberl & Hower, 1976) and second (Huang et al., 1993) to higher orders (e.g., 5th order from Pytte & Reynolds, 1989, but a higher order is more appropriate for reproducing the full range of the S–I reaction in sedimentary basins (Altaner, 1989; Cuadros, 2006). Kinetic modeling of progression of the S–I reaction in the

Nankai margin has shown that the equation of Pytte and Reynolds (1989) yields better results than that of Huang et al. (1993) (Saffer & McKiernan, 2009; Saffer et al., 2008). Thus, as our starting equation, we adopted the rate law proposed by Pytte and Reynolds (1989):

$$-\frac{dS}{dt} = S^a \left(\frac{\mathrm{K}}{\mathrm{Na}}\right)^b A \exp\left(-\frac{E_a}{RT}\right), \tag{4.1}$$

where S is the smectite fraction in I/S; a and b are the reaction orders ($a = 5, b = 1$); t is time in seconds; K and Na are the activities of potassium and sodium, respectively; A is the frequency factor ($5.2 \times 10^7\ \mathrm{s}^{-1}$); E_a is the activation energy for the reaction (33 kcal mol^{-1}~138 kJ mol^{-1}); T is the temperature in Kelvin; and R is the gas constant (~8.314 J K^{-1} mol^{-1}). We adopted results from pore-water chemical analyses for K and Na (8.2 mM and 570 mM, respectively; Expedition 316 Scientists, 2009). Equation (4.1) is integrated with the initial condition of $S = S_0$ at $t = 0$:

$$S = \left[\frac{1}{{S_0}^4} + 4A\left(\frac{\mathrm{K}}{\mathrm{Na}}\right)\int_0^t \exp\left(-\frac{E_a}{RT}\right) dt\right]^{-\frac{1}{4}}. \tag{4.2}$$

We used the temperature–time history constructed by Hamada et al. (2015) and Hamada (2013) to solve equation (4.2). The authors estimated a maximum temperature of ~330 °C for the Nankai megasplay fault and ~410 °C for the Shirako Fault. We calculated $\%I$ as follows:

$$\%I = 100 \times (1 - S). \tag{4.3}$$

Following Vrolijk and van der Pluijm (1999), the activation energy E_a of equations (4.1) and (4.2) was adjusted to reproduce the observed S–I reaction in the fault zone. As well as determining the sensitivity of the apparent activation energy, we calculated the cumulative effect of a number of repeated same slip events for activation energy of 138 kJ mol^{-1}.

4.3 Results

4.3.1 Clay mineral analysis using XRD

Figures 4.1 and 4.2 show EG XRD patterns for the gouge and host sediment samples. The peaks indicate that all the samples contain the same mineral phases, including I/S, discrete illite, and chlorite + kaolinite. The peak positions suggest that I/S is a randomly interstratified (R0) phase (Reynolds, 1980; D. M. Moore & Reynolds, 1997). Although the profiles are largely similar, the saddle-to-peak intensity ratio of the I/S 001 is markedly higher in the gouge sample (28R-2-038) than in the host sediment samples, indicating higher $\%I$ (Weir et al., 1975). This is consistent with the result of Yamaguchi et al. (2011).

The results of quantitative XRD analysis are summarized in Figure 4.3 and Table 4.1. For comparison, data from Guo and Underwood (2012) for the same depth interval are plotted. The $\%I$ value for the host sediments is $34.5 \pm 7.5\%$, which is comparable to the previous data ($36 \pm 3\%$), whereas the $\%I$ of the gouge is 48.7%, much higher than that of the host. For the host sediment samples, the relative weight proportions of smectite, illite, and chlorite + kaolinite are 36.9 ± 7.9%, 41.4 ± 7.1%, and 21.7 ± 5.0%, respectively. There is no discrepancy between our results and previous findings, except that the gouge sample shows a lower smectite content and slightly higher illite content compared with the host sediments. This is likely to be an apparent effect of the decrease in I/S 001 peak intensity due to the progression of illitization. The full width at half maximum (FWHM) of the I001 peak for the gouge sample (0.38) is slightly larger than the average for host sediments (0.35 ± 0.03), but is within two standard deviations (2σ) (Table 4.1).

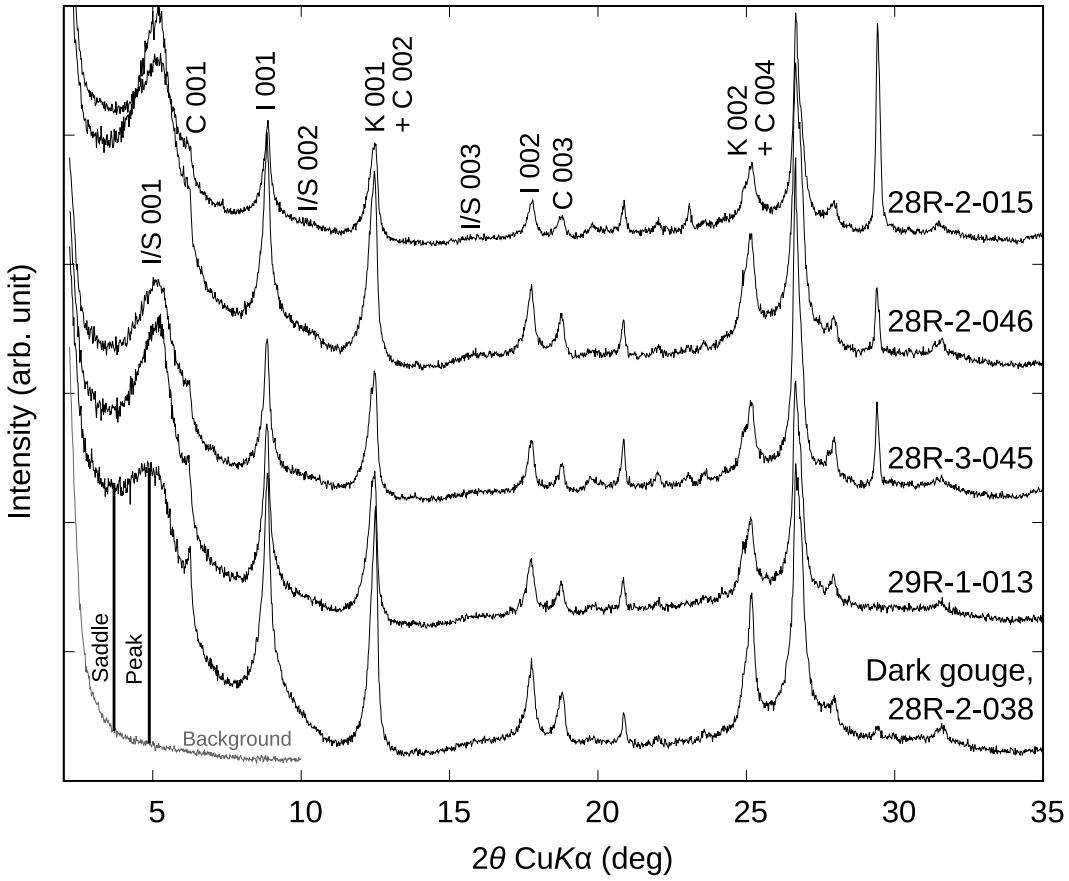

Figure 4.1: Selected X-ray diffraction patterns for the ethylene-glycolate-treated clay fraction (<2 µm) of C0004 Site sediments, including dark gouge samples. I, illite; S, smectite; C, chlorite; K, kaolinite. The saddle and peak of I/S 001 are shown for the dark gouge pattern. The "background" pattern is for a glass slide.

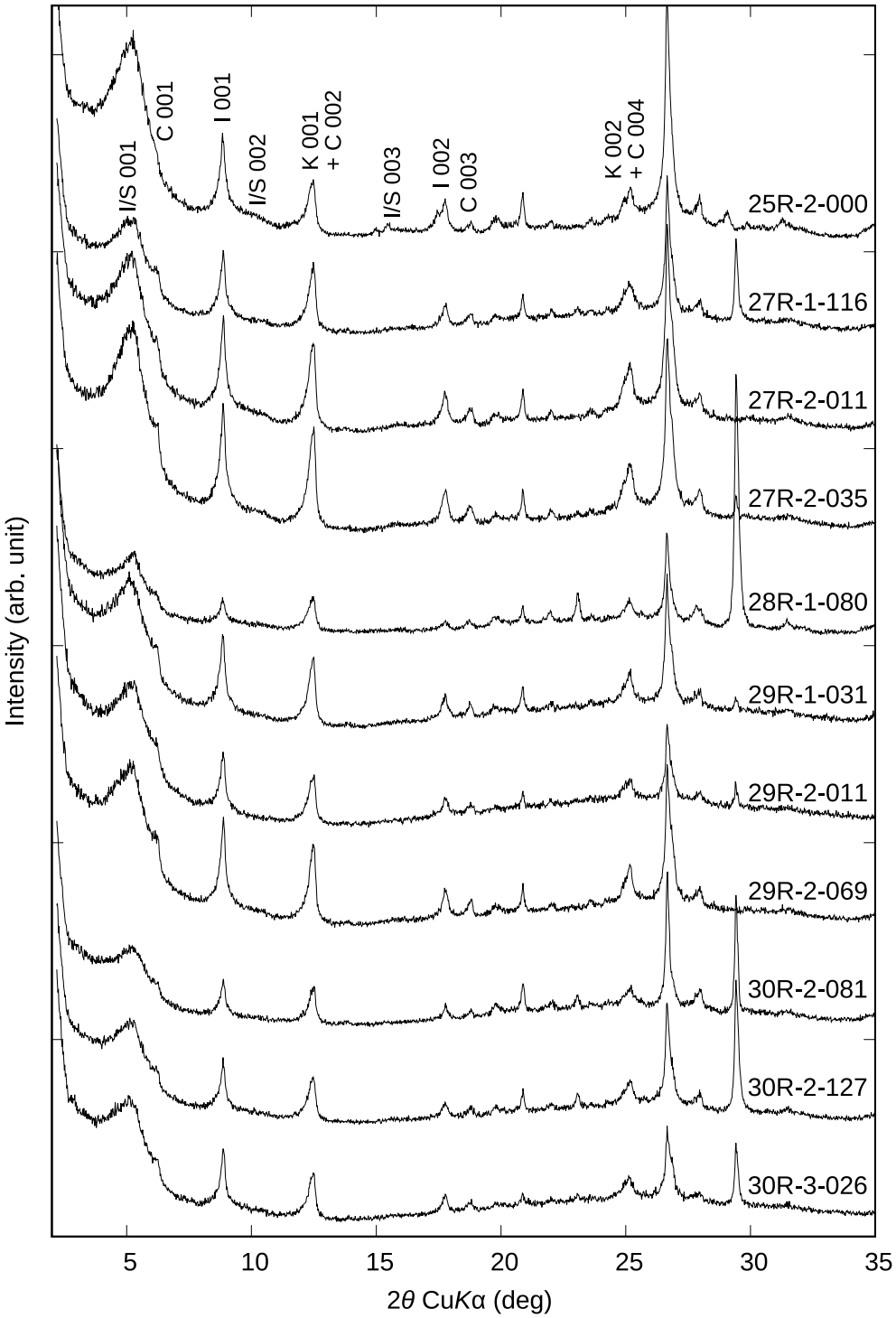

Figure 4.2: X-ray diffraction patterns for the ethylene-glycolate-treated clay fraction (<2 μm) of host sediments of C0004 Site. I, illite; S, smectite; C, chlorite; K, kaolinite.

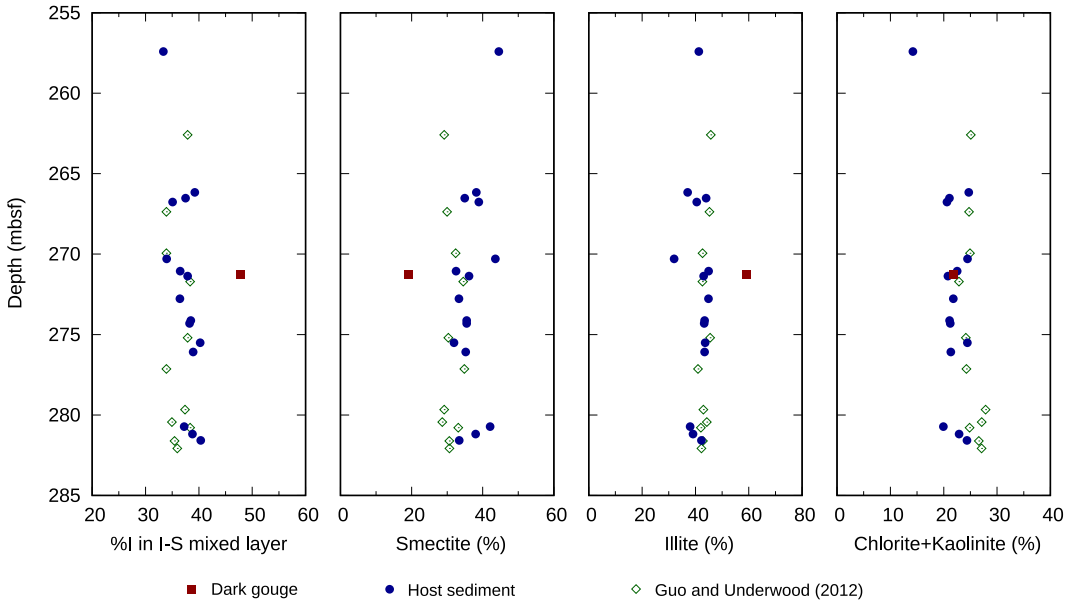

Figure 4.3: Depth (mbsf) versus $\%I$ in mixed-layer illite/smectite using Biscaye (1965) weighted peak-area percentages for smectite, illite, and chlorite + kaolinite. The results of Guo and Underwood (2012) are also shown.

Table 4.1: Peak data for illite–smectite 001, illite 001, and kaolinite 001 + chlorite 002. The values of $\%I$ in mixed-layer illite/smectite were estimated using the working curve of Inoue et al. (1989). The peak-area percentages were calculated using the weighting factors of Biscaye (1965): 1 × area of smectite 001, 4 × illite 001, and 2 × (kaolinite 001 + chlorite 002).

		I-S mixed layer		Peak area			Biscaye peak-area percentages			FWHM
Sample name	Depth (mbsf)	Saddle/peak	$\%I$ in I-S mixed layer	Smectite 001	Illite 001	Kaolinite 001 + chlorite 002	Smectite (%)	Illite (%)	chlorite (%)	Illite 001
25R-2-000	257.41	0.530	32.4	77817	18027	12435	44.5	41.3	14.2	0.36
27R-1-116	266.16	0.495	30.5	51836	12586	16752	38.2	37.1	24.7	0.34
27R-2-011	266.52	0.641	38.0	62123	19555	18733	34.9	44.0	21.1	0.34
27R-2-035	266.76	0.580	35.0	77928	20285	20660	38.9	40.5	20.6	0.33
28R-1-080	270.30	0.529	32.3	31763	5834	8921	43.5	32.0	24.5	0.38
28R-2-015	271.06	0.612	36.5	46133	15943	15982	32.5	45.0	22.5	0.35
28R-2-038 (dark gouge)	**271.29**	**0.902**	**48.7**	**58597**	**45166**	**33324**	**19.2**	**59.1**	**21.8**	**0.38**
28R-2-046	271.37	0.564	34.1	107978	32182	31045	36.1	43.1	20.8	0.35
28R-3-045	272.77	0.557	33.8	61810	20839	20223	33.3	44.9	21.8	0.33
29R-1-013	274.13	0.635	37.6	83749	25635	24890	35.5	43.4	21.1	0.34
29R-1-031	274.31	0.641	37.9	46350	14122	13859	35.5	43.3	21.2	0.33
29R-2-011	275.51	0.498	30.6	34702	11860	13283	31.9	43.6	24.4	0.35
29R-2-069	276.09	0.662	38.9	52243	16115	15815	35.2	43.5	21.3	0.32
30R-2-081	280.72	0.521	31.9	34044	7690	8064	42.1	38.0	19.9	0.38
30R-2-127	281.18	0.440	27.4	36655	9425	11029	38.0	39.1	22.9	0.35
30R-3-026	281.58	0.706	40.9	30561	9674	11150	33.4	42.3	24.4	0.36
Average of host sediment		0.574	34.5				36.9	41.4	21.7	0.35
2σ		0.148	7.5				7.9	7.1	5.0	0.03
26R-3, 0*	262.59	0.64	38	33554	13173	14433	29.1	45.8	25.1	
27R-2, 95*	267.37	0.56	34	52425	19769	21630	30.0	45.2	24.8	
28R-1, 43*	269.94	0.56	34	57507	18947	22138	32.4	42.7	24.9	
28R-2, 80*	271.71	0.65	38	39594	12214	13096	34.5	42.6	22.8	
29R-1, 120*	275.20	0.64	38	42421	15910	16877	30.3	45.5	24.1	
29R-CC, 18*	277.14	0.56	34	51082	15019	17795	34.8	40.9	24.3	
30R-1, 117*	279.67	0.63	37	37658	13870	17983	29.2	43.0	27.9	
30R-2, 53*	280.44	0.58	35	37933	14673	17982	28.6	44.3	27.1	
30R-2, 88*	280.79	0.65	38	45729	14515	17159	33.1	42.0	24.8	
30R-3, 29*	281.61	0.59	35	49680	17376	21581	30.6	42.8	26.6	
30R-3, 76*	282.08	0.60	36	35202	12126	15565	30.7	42.2	27.1	
32R-2, 120*	290.11	0.57	34	43839	16233	17636	30.4	45.1	24.5	
34R-1, 15*	296.65	0.64	38	45956	14431	16795	33.5	42.1	24.5	
36R-2, 0*	306.69	0.59	35	49598	14724	16979	34.8	41.3	23.8	

*Data from Guo and Underwood (2012).

4.3.2 Calibration of apparent activation energy for the S–I reaction in seismogenic faults

Figure 4.4a shows a best-fit solution for the evolution of temperature associated with seismic slip along the megasplay fault in the Nankai Trough (Hamada et al., 2015) and the corresponding progression of the S–I reaction fostered by this heating event. Figure 4.5a and b shows the results of our S–I reaction modeling with different activation energies. The reaction hardly progresses with the original value of E_a (~138 kJ mol^{-1}); however, the reaction shows greater progression with lower activation energies. As a result, E_a =100 kJ mol^{-1} can reasonably explain the reaction progression (Figures 4.4a and 4.5a). In the case of the Shirako Fault, E_a =110 kJ mol^{-1} can reproduce the S–I reaction progression (Figures 4.4b and 4.5b). The relationship between $\%I$ and the number of slip events indicates that cumulative slip events assist the progression of the S–I reaction (Figure 4.5c and d). However, even 10^3 repeated slip events cannot raise $\%I$ to the observed value of the dark gouge of the Nankai megasplay fault (Figure 4.5c). In the case of the Shirako Fault, the reaction cannot be attained within the acceptable range of the total slip distance (<500 m; Kameda et al., 2013).

4.4 Discussions

Although the degree of progression of the S–I reaction was not estimated by Yamaguchi et al. (2011), our XRD analysis shows that it is ~14$\%I$ relative to the host sediments (Figure 4.3; Table 4.1). However, based on the thermal model of Hamada et al. (2015), such reaction progression is not explained by the kinetics reported by Pytte and Reynolds (1989) (Figure 4.4). A similar discrepancy was also found by Hirono et al. (2014). Hirono et al. (2009) investigated the Nankai megasplay fault samples using multiple geothermometers but detected no temperature signal, on which basis Hirono et al. (2014) subsequently concluded that the megasplay fault has not experienced fluid–rock interaction at temperatures of ≥250 °C. Hirono et al. (2014) further examined the feasibility of the S–I reaction progression with

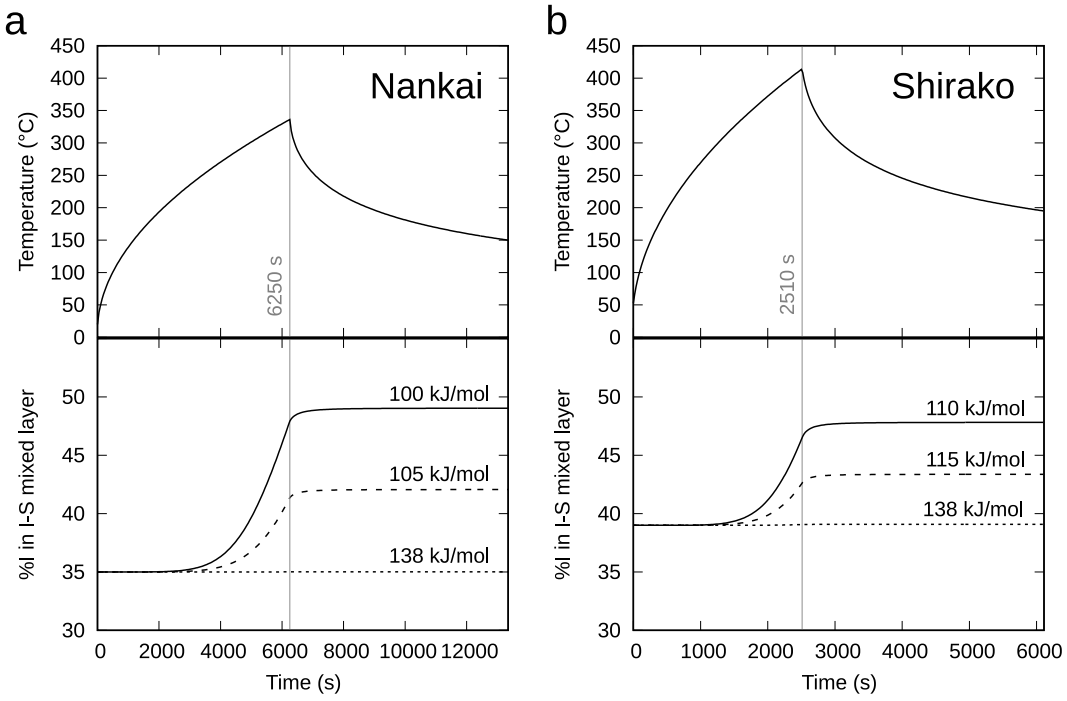

Figure 4.4: Temporal evolution of temperature with time and $\%I$ in mixed-layer illite/smectite during a simulated slip event upon (a) the megasplay fault in the Nankai Trough and (b) the Shirako Fault in the Miura–Boso accretionary prism. The results of the calibration of apparent activation energy for the S–I reaction are shown in the lower panels. The activation energy of 138 kJ mol^{-1} is from Pytte and Reynolds (1989).

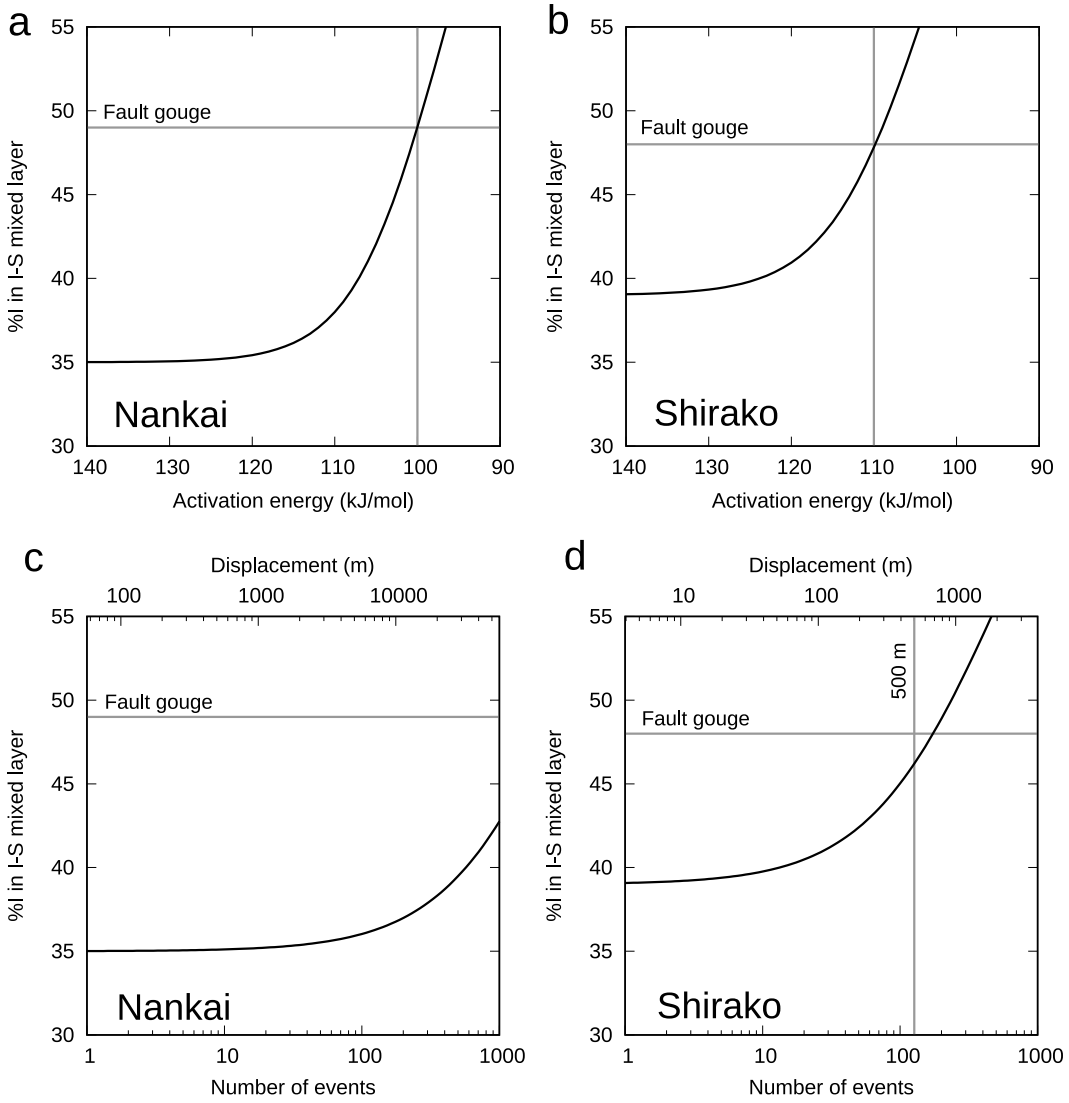

Figure 4.5: Sensitivity of $\%I$ in mixed-layer illite/smectite to the activation energy of illitization, and the sensitivity of $\%I$ in mixed-layer illite/smectite to the number of repeated slip events. The calculated $\%I$ variation with respect to activation energy is shown for (a) the megasplay fault in the Nankai Trough and (b) the Shirako Fault. The calculated $\%I$ variation with respect to the number of slip events and corresponding displacement is shown for (c) the megasplay fault in the Nankai Trough and (d) the Shirako Fault. Observations for fault gouges are shown in each panel. The line marking 500 m for the Shirako Fault indicates the total displacement along the thrust system in the vicinity of the fault.

this temperature constraint and discovered that reaction progression is unlikely under high-velocity slip ($1\,m\,s^{-1}$). Therefore, slow and long-term slip may have occurred on the megasplay fault. Hamada et al. (2015) reported a best-fit solution for vitrinite reflectance using a slip velocity of $0.91\,cm\,s^{-1}$ and a slip distance of 56.7 m, and their solution yielded a maximum temperature of ~330 °C.

Based on the temperature model to reproduce vitrinite reflectance anomaly (Hamada, 2013; Hamada et al., 2015), the observed S–I reaction along the Nankai megasplay fault is explained by an apparent activation energy of $100\,kJ\,mol^{-1}$ (Figure 4.5a), whereas the reaction on the Shirako Fault is reproduced with an apparent activation energy of $110\,kJ\,mol^{-1}$ (Figure 4.5b). This difference in activation energy is due to a larger $\%I$ anomaly on the megasplay fault (~14%) than on the Shirako Fault (~9%). In addition, the difference in rise time (6250 s for the Nankai megasplay fault, 2510 s for the Shirako Fault) affects the apparent activation energy. It has been suggested that the cumulative effect of repeated slip events may also affect the progression of the S–I reaction. For instance, Fulton and Harris (2012) demonstrated that the vitrinite reflectance anomaly within the megasplay fault could reflect the accumulation of more than 10^2 slip events. However, our result shows that even 10^3 events are insufficient to explain the observed $\%I$ increase (Figure 4.5c). For the Shirako Fault, repeated slip also cannot reproduce the $\%I$ anomaly in the fault gouge, as the amount of slip needed exceeds the upper bound of the total slip distance (Figure 4.5d; Kameda et al., 2013). Therefore, our results indicate that the progression of the S–I reaction may require modification of the reaction kinetics associated with faulting, as outlined below.

In general, the S–I reaction is considered to be a thermally activated process (e.g. Perry & Hower, 1970), but in a dynamic environment such as a fault zone it is possible that the reaction could be promoted by a faulting-assisted overcoming of the kinetic barrier possibly due to the destruction of parent crystals in the solid-state transformation process. On the other hand, Hirono et al. (2014) argued that the S–I reaction in the Nankai megasplay fault might be promoted by a comminution–dissolution–recrystallization process during earthquake slip, which may also contribute to the reduction in the apparent activation energy of the

reaction. The S–I reaction is also facilitated by K^+ enriched fluid (e.g. Eberl & Hower, 1976; Whitney & Northrop, 1988). The comminution and dissolution of minerals in the fault zone can increase the K^+ concentration in the pore fluid, but the process concurrently supply other elements such as Ca^{2+}, Mg^{2+}, or Na^+, which in turn inhibit the reaction progress (Huang et al., 1993; Roberson & Lahann, 1981). It is therefore supposed that the mechanochemical enhancement of the reaction is more likely in the relevant fault zones. A friction experiment on illite gouge by Hirono et al. (2013) showed that frictional faulting increasingly damages the crystal structure of illite with increases in frictional energy density [= integration of (shear stress × slip displacement / thickness of sample)]. In addition, those authors demonstrated that the activation energy of the dehydroxylation reaction decreases by ~32% when ~18 MJ m^{-3} of frictional energy density is applied. Based on these arguments, it is expected that the kinetic barrier of the S–I reaction is also lowered by faulting in the Nankai megasplay and the Shirako slip zones. Our kinetic modeling shows that a ~20–30% decrease in the literature-reported activation energy yields a result consistent with the observed illitization. Although the decrease in the activation energy is similar to the experimental result of Hirono et al. (2013), it should be noted that the frictional energy density of the Nankai slip is as much as ~10^4 MJ m^{-3} (Hamada et al., 2015), which is almost three orders of magnitude greater than the experimental observation. One reason for this discrepancy may be a difference in the susceptibility of the two reactions (i.e., dehydroxylation and the transformation reaction) to mechanical damage. In addition, the friction experiment was carried out under dry conditions, and the associated dehydroxylation reaction may progress more favorably than under natural water-saturated conditions, which may lead to an overestimate of the mechanical damage. Further examples are necessary to address these issues and to construct more reliable kinetics applicable to fault zones.

4.5 Conclusions

We proposed a modified kinetic model to explain the local progression of smectite-to-illite conversion within Nankai megasplay fault gouge and Shirako Fault gouge. The thermal histories associated with coseismic slips obtained from vitrinite reflectance analyses indicate that the apparent activation energy of the S–I reaction is reduced by ~20%–30% compared with the static condition. This result suggests that the kinetic barrier of the S–I reaction is lowered by a mechanochemical effect in seismogenic fault zones.

References

Aglietti, E., Porto Lopez, J., & Pereira, E. (1986). Mechanochemical effects in kaolinite grinding. I. Textural and physicochemical aspects. *International Journal of Mineral Processing*, *16*(1–2), 125–133. doi: 10.1016/0301-7516(86)90079-7

Ahn, J. H., & Peacor, D. R. (1986). Transmission and analytical electron microscopy of the smectite-to-illite transition. *Clays and Clay Minerals*, *34*(2), 165–179. doi: 10.1346/CCMN.1986.0340207

Altaner, S. P. (1989). Calculation of K diffusional rates in bentonite beds. *Geochimica et Cosmochimica Acta*, *53*(4), 923–931. doi: 10.1016/0016-7037(89)90037-9

Altaner, S. P., & Ylagan, R. F. (1997). Comparison of structural models of mixed-layer illite/smectite and reaction mechanisms of smectite illitization. *Clays and Clay Minerals*, *45*(4), 517–533. doi: 10.1346/CCMN.1997.0450404

Ando, M. (1975). Source mechanisms and tectonic significance of historical earthquakes along the nankai trough, Japan. *Tectonophysics*, *27*(2), 119–140. doi: 10.1016/0040-1951(75)90102-X

Baba, T., & Cummins, P. R. (2005). Contiguous rupture areas of two Nankai Trough earthquakes revealed by high-resolution tsunami waveform inversion. *Geophysical Research Letters*, *32*(8), L08305. doi: 10.1029/2004GL022320

Baba, T., Cummins, P. R., Hori, T., & Kaneda, Y. (2006). High precision slip distribution of the 1944 Tonankai earthquake inferred from tsunami waveforms: Possible slip on a splay fault. *Tectonophysics*, *426*(1–2), 119–134. doi: 10.1016/j.tecto.2006.02.015

Bailey, S. W. (1980). Structures of layer silicates. In G. W. Brindley & G. Brown (Eds.), *Crystal structures of clay minerals and their x-ray identification* (pp. 1–124). London: Mineralogical Society.

Bellotto, M., Gualtieri, A., Artioli, G., & Clark, S. M. (1995). Kinetic study of the kaolinite-mullite reaction sequence. Part I: Kaolinite dehydroxylation. *Physics and Chemistry of Minerals*, *22*(4), 207–217. doi: 10.1007/BF00202253

Bethke, C. M., & Altaner, S. P. (1986). Layer-by-layer mechanism of smectite illitization and application to a new rate law. *Clays and Clay Minerals*, *34*(2), 136–145. doi: 10.1346/CCMN.1986.0340204

Biscaye, P. E. (1965). Mineralogy and sedimentation of recent deep-sea clay in the Atlantic ocean and adjacent seas and oceans. *Geological Society of America Bulletin*, *76*(7), 803–832. doi: 10.1130/0016-7606(1965)76[803:MASORD]2.0.CO;2

Bish, D. L., & von Dreele, R. B. (1989). Rietveld refinement of non-hydrogen atomic positions in kaolinite. *Clays and Clay Minerals*, *37*(4), 289–296. doi: 10.1346/CCMN.1989.0370401

Boles, J. R., & Franks, S. G. (1979). Clay diagenesis in Wilcox sandstones of Southwest Texas: Implications of smectite diagenesis on sandstone cementation. *Journal of Sedimentary Research*, *49*(1), 55–70. doi: 10.1306/212F76BC-2B24-11D7-8648000102C1865D

Brandt, F., Bosbach, D., Krawczyk-Barsch, E., Arnold, T., & Bernhard, G. (2003). Chlorite dissolution in the acid ph-range: A combined microscopic and macroscopic approach. *Geochimica et Cosmochimica Acta*, *67*(8), 1451–1461. doi: 10.1016/S0016-7037(02)01293-0

Brindley, G. W., & Ali, S. (1950). X-Ray study of thermal transformations in some magnesian chlorite minerals. *Acta Crystallographica*, *3*(1), 25–30. doi: 10.1107/S0365110X50000069

Brindley, G. W., & Chang, T. (1974). Development of long basal spacings in chlorites by thermal treatment. *American Mineralogist*, *59*(1962), 152–158.

Brindley, G. W., & Nakahira, M. (1957). Kinetics of dehydroxylation of kaolinite and halloysite. *Journal of the American Ceramic Society*, *40*(10), 346–350. doi:

10.1111/j.1151-2916.1957.tb12549.x

Burst Jr., J. F. (1957). Postdiagenetic clay mineral environmental relationships in the Gulf Coast Eocene. *Clays and Clay Minerals*, *6*(1), 327–341. doi: 10.1346/CCMN.1957.0060124

Caillère, M. S., & Hénin, S. (1957). The chlorite and serpentine minerals. In R. C. Mackenzie (Ed.), *The differential thermal investigation of clays* (pp. 207–230). London: Mineralogical Society.

Carslaw, H. S., & Jaeger, J. C. (1959). *Conduction of heat in solids* (2nd ed.). Oxford: Clarendon Press.

Criado, J. M., Ortega, A., Real, C., & Torres de Torres, E. (1984). Re-Examination of the Kinetics of the Thermal Dehydroxylation of Kaolinite. *Clay Minerals*, *19*(4), 653–661. doi: 10.1180/claymin.1984.019.4.11

Cuadros, J. (2006). Modeling of smectite illitization in burial diagenesis environments. *Geochimica et Cosmochimica Acta*, *70*(16), 4181–4195. doi: 10.1016/j.gca.2006.06.1372

Cuadros, J. (2012). Clay crystal-chemical adaptability and transformation mechanisms. *Clay Minerals*, *47*(2), 147–164. doi: 10.1180/claymin.2012.047.2.01

Cuadros, J., & Altaner, S. P. (1998). Characterization of mixed-layer illite-smectite from bentonites using microscopic, chemical, and X-ray methods: Constraints on the smectite-to-illite transformation mechanism. *American Mineralogist*, *83*(7–8), 762–774. doi: 10.2138/am-1998-7-808

Cuadros, J., & Linares, J. (1996). Experimental kinetic study of the smectite-to-illite transformation. *Geochimica et Cosmochimica Acta*, *60*(3), 439–453. doi: 10.1016/0016-7037(95)00407-6

Eberl, D., & Hower, J. (1976). Kinetics of illite formation. *Geological Society of America Bulletin*, *87*(9), 1326–1330. doi: 10.1130/0016-7606(1976)87<1326:KOIF>2.0.CO;2

Elliott, W. C., Aronson, J. L., Matisoff, G., & Gautier, D. L. (1991). Kinetics of the smectite to illite transformation in the Denver Basin: Clay mineral, K-Ar data, and mathematical model results. *American Association of*

Petroleum Geologists Bulletin, *75*(3), 436–462. doi: 10.1306/0C9B2803-1710-11D7-8645000102C1865D

Expedition 316 Scientists. (2009). Expedition 316 Site C0004. In M. Kinoshita et al. (Eds.), *Proceedings of the integrated ocean drilling program* (Vol. 314/315/316). Integrated Ocean Drilling Program Management International, Inc. doi: 10.2204/iodp.proc.314315316.133.2009

Földvári, M. (2011). *Handbook of thermogravimetric system of minerals and its use in geological practice, occasional papers of the geological institute of hungary* (Vol. 213). Budapest: Geological Institute of Hungary.

Franco, F., Pérez-Maqueda, L., & Pérez-Rodríguez, J. (2003). The influence of ultrasound on the thermal behaviour of a well ordered kaolinite. *Thermochimica Acta*, *404*(1-2), 71–79. doi: 10.1016/S0040-6031(03)00065-0

Friedman, H. L. (1964). Kinetics of thermal degradation of char–forming plastics from thermogravimetry. Application to a phenolic plastic. *Journal of Polymer Science: Polymer Symposia*, *6*(1), 183–195. doi: 10.1002/polc.5070060121

Frost, R. L., Makó, É., Kristóf, J., Horváth, E., & Kloprogge, J. T. (2001). Mechanochemical treatment of kaolinite. *Journal of Colloid and Interface Science*, *239*(2), 458–466. doi: 10.1006/jcis.2001.7591

Fujiwara, T., Kodaira, S., No, T., Kaiho, Y., Takahashi, N., & Kaneda, Y. (2011). The 2011 Tohoku-Oki earthquake: Displacement reaching the trench axis. *Science*, *334*(6060), 1240–1240. doi: 10.1126/science.1211554

Fulton, P. M., Brodsky, E. E., Kano, Y., Mori, J., Chester, F., Ishikawa, T., … Expedition 343, 343T, and KR13-08 Scientists (2013). Low Coseismic Friction on the Tohoku-Oki Fault Determined from Temperature Measurements. *Science*, *342*(6163), 1214–1217. doi: 10.1126/science.1243641

Fulton, P. M., & Harris, R. N. (2012). Thermal considerations in inferring frictional heating from vitrinite reflectance and implications for shallow coseismic slip within the Nankai Subduction Zone. *Earth and Planetary Science Letters*, *335-336*, 206–215. doi: 10.1016/j.epsl.2012.04.012

Gailhanou, H., Rogez, J., van Miltenburg, J. C., van Genderen, A. C. G., Grenèche, J. M., Gilles, C., … Blanc, P. (2009). Thermodynamic properties of

chlorite CCa-2. Heat capacities, heat contents and entropies. *Geochimica et Cosmochimica Acta*, *73*(16), 4738–4749. doi: 10.1016/j.gca.2009.04.040

Girgis, B. S., Felix, N. S., & El-Barawy, K. A. (1987). Dehydroxylation kinetics of some pure smectites. *Thermochimica Acta*, *112*(2), 265–274. doi: 10.1016/0040-6031(87)88283-7

Grim, R. E. (1968). Dehydration, rehydration, and the changes taking place on heating. In *Clay mineralogy* (2nd ed., pp. 278–352). New York: McGraw-Hill.

Gualtieri, A. F., & Ferrari, S. (2006). Kinetics of illite dehydroxylation. *Physics and Chemistry of Minerals*, *33*(7), 490–501. doi: 10.1007/s00269-006-0092-z

Guggenheim, S., & Zhan, W. (1999). Crystal structures of two partially dehydrated chlorites: The "modified" chlorite structure. *American Mineralogist*, *84*(9), 1415–1421. doi: 10.2138/am-1999-0920

Güler, Ç., & Sarier, N. (1990). Kinetics of the thermal dehydration of acid-activated montmorillonite by the rising temperature technique. *Thermochimica Acta*, *159*, 29–33. doi: 10.1016/0040-6031(90)80090-L

Guo, J., & Underwood, M. (2012). Data report: clay mineral assemblages from the Nankai Trough accretionary prism and the Kumano Basin, IODP Expeditions 315 and 316, NanTroSEIZE Stage 1. In M. Kinoshita et al. (Eds.), *Proceedings of the integrated ocean drilling program* (Vol. 314/315/316). Washington, DC: Integrated Ocean Drilling Program Management International, Inc. doi: 10.2204/iodp.proc.314315316.202.2012

Hamada, Y. (2013). *Investigation of slip parameters and fault slip behavior in the shallow part of subduction zone on the basis of vitrinite reflectance* (Unpublished doctoral dissertation). The University of Tokyo.

Hamada, Y., Hirono, T., & Ishikawa, T. (2011). Coseismic frictional heating and fluid-rock interaction in a slip zone within a shallow accretionary prism and implications for earthquake slip behavior. *Journal of Geophysical Research*, *116*(B1), B01302. doi: 10.1029/2010JB007730

Hamada, Y., Sakaguchi, A., Tanikawa, W., Yamaguchi, A., Kameda, J., & Kimura, G. (2015). Estimation of slip rate and fault displacement during shallow earthquake rupture in the Nankai subduction zone. *Earth, Planets and Space*,

67, 39. doi: 10.1186/s40623-015-0208-0

Hanamura, Y., & Ogawa, Y. (1993). Layer-parallel faults, duplexes, imbricate thrusts and vein structures of the Miura Group: Keys to understanding the Izu fore-arc sediment accretion to the Honshu fore arc. *Island Arc*, *2*(3), 126–141. doi: 10.1111/j.1440-1738.1993.tb00081.x

Hirono, T., Fujimoto, K., Yokoyama, T., Hamada, Y., Tanikawa, W., Tadai, O., … Song, S. R. (2008). Clay mineral reactions caused by frictional heating during an earthquake: An example from the Taiwan Chelungpu fault. *Geophysical Research Letters*, *35*(16), L16303. doi: 10.1029/2008GL034476

Hirono, T., & Ishikawa, T. (2018). Tectono-seismic characteristics of faults in the shallow portion of an accretionary prism. *Tectonophysics*, *724-725*, 179–194. doi: 10.1016/j.tecto.2018.01.014

Hirono, T., Ishikawa, T., Masumoto, H., Kameda, J., Yabuta, H., & Mukoyoshi, H. (2014). Re-evaluation of frictional heat recorded in the dark gouge of the shallow part of a megasplay fault at the Nankai Trough. *Tectonophysics*, *626*, 157–169. doi: 10.1016/j.tecto.2014.04.020

Hirono, T., Maekawa, Y., & Yabuta, H. (2015). Investigation of the records of earthquake slip in carbonaceous materials from the Taiwan Chelungpu fault by means of infrared and Raman spectroscopies. *Geochemistry, Geophysics, Geosystems*, *16*(5), 1233–1253. doi: 10.1002/2014GC005622

Hirono, T., & Tanikawa, W. (2011). Implications of the thermal properties and kinetic parameters of dehydroxylation of mica minerals for fault weakening, frictional heating, and earthquake energetics. *Earth and Planetary Science Letters*, *307*(1–2), 161–172. doi: 10.1016/j.epsl.2011.04.042

Hirono, T., Tanikawa, W., Honda, G., Kameda, J., Fukuda, J., & Ishikawa, T. (2013). Importance of mechanochemical effects on fault slip behavior during earthquakes. *Geophysical Research Letters*, *40*(12), 2988–2992. doi: 10.1002/grl.50609

Hirono, T., Ujiie, K., Ishikawa, T., Mishima, T., Hamada, Y., Tanimizu, M., … Kinoshita, M. (2009). Estimation of temperature rise in a shallow slip zone of the megasplay fault in the Nankai Trough. *Tectonophysics*, *478*(3–4), 215–220.

doi: 10.1016/j.tecto.2009.08.001

Honda, G., Ishikawa, T., Hirono, T., & Mukoyoshi, H. (2011). Geochemical signals for determining the slip-weakening mechanism of an ancient megasplay fault in the Shimanto accretionary complex. *Geophysical Research Letters*, *38*(6), L06310. doi: 10.1029/2011GL046722

Howard, J. J., & Roy, D. M. (1985). Development of Layer Charge and Kinetics of Experimental Smectite Alteration. *Clays and Clay Minerals*, *33*(2), 81–88. doi: 10.1346/CCMN.1985.0330201

Hower, J., Eslinger, E. V., Hower, M. E., & Perry, E. A. (1976). Mechanism of burial metamorphism of argillaceous sediment: 1. Mineralogical and chemical evidence. *Geological Society Of America Bulletin*, *87*(5), 725–737. doi: 10.1130/0016-7606(1976)87<725

Huang, W.-L., Longo, J. M., & Pevear, D. R. (1993). An experimentally derived kinetic model for smectite-to-illite conversion and its use as a geothermometer. *Clays and Clay Minerals*, *41*(2), 162–177. doi: 10.1346/CCMN.1993.0410205

Ichinose, G. A., Thio, H. K., Somerville, P. G., Sato, T., & Ishii, T. (2003). Rupture process of the 1944 Tonankai earthquake (M_s 8.1) from the inversion of teleseismic and regional seismograms. *Journal of Geophysical Research*, *108*(B10), 2497. doi: 10.1029/2003JB002393

Ikari, M. J., Saffer, D. M., & Marone, C. (2009). Frictional and hydrologic properties of a major splay fault system, Nankai subduction zone. *Geophysical Research Letters*, *36*(20), L20313. doi: 10.1029/2009GL040009

Ikesawa, E., Sakaguchi, A., & Kimura, G. (2003). Pseudotachylyte from an ancient accretionary complex: Evidence for melt generation during seismic slip along a master décollement? *Geology*, *31*(7), 637–640. doi: 10.1130/0091-7613(2003)031<0637:PFAAAC>2.0.CO;2

Inoue, A. (1987). Chemical and morphological evidence for the conversion of smectite to illite. *Clays and Clay Minerals*, *35*(2), 111–120. doi: 10.1346/CCMN.1987.0350203

Inoue, A., Bouchet, A., Velde, B., & Meunier, A. (1989). Convenient tech-

nique for estimating smectite layer percentage in randomly interstratified illite/smectite minerals. *Clays and Clay Minerals*, *37*(3), 227–234. doi: 10.1346/CCMN.1989.0370305

Inoue, A., Utada, M., & Wakita, K. (1992). Smectite-to-illite conversion in natural hydrothermal systems. *Applied Clay Science*, *7*(1-3), 131–145. doi: 10.1016/0169-1317(92)90035-L

Ishikawa, T., Tanimizu, M., Nagaishi, K., Matsuoka, J., Tadai, O., Sakaguchi, M., … Song, S.-R. (2008). Coseismic fluid-rock interactions at high temperatures in the Chelungpu fault. *Nature Geoscience*, *1*(10), 679–683. doi: 10.1038/ngeo308

Ito, Y., Tsuji, T., Osada, Y., Kido, M., Inazu, D., Hayashi, Y., … Fujimoto, H. (2011). Frontal wedge deformation near the source region of the 2011 Tohoku-Oki earthquake. *Geophysical Research Letters*, *38*(15), L00G05. doi: 10.1029/2011GL048355

Kameda, J., Yamamoto, Y., Hamada, Y., Fujimoto, K., & Kimura, G. (2013). Progress of illitization along an imbricate frontal thrust at shallow depths in an accretionary prism. *Tectonophysics*, *600*, 41–51. doi: 10.1016/j.tecto.2013.04.024

Kaneki, S., Hirono, T., Mukoyoshi, H., Sampei, Y., & Ikehara, M. (2016). Organochemical characteristics of carbonaceous materials as indicators of heat recorded on an ancient plate-subduction fault. *Geochemistry, Geophysics, Geosystems*, *17*(7), 2855–2868. doi: 10.1002/2016GC006368

Kaneki, S., Ichiba, T., & Hirono, T. (2018). Mechanochemical effect on maturation of carbonaceous material: Implications for thermal maturity as a proxy for temperature in estimation of coseismic slip parameters. *Geophysical Research Letters*, *45*(5), 2248–2256. doi: 10.1002/2017GL076791

Kawakami, S. (2001). Upper miocene radiolarians from the nishizaki formation and ishido group in the southern part of boso peninsula, japan, and their geological significance (in japanese with english abstract). *News of Osaka Micropaleontlogists Special Volume*, *12*, 343–358.

Khawam, A., & Flanagan, D. R. (2006). Solid-state kinetic models: basics and

mathematical fundamentals. *The Journal of Physical Chemistry B*, *110*(35), 17315–17328. doi: 10.1021/jp062746a

Kimura, G., Screaton, E. J., Curewitz, D., & the Expedition 316 Scientists. (2008). *NanTroSEIZE stage 1A: NanTroSEIZE shallow megasplay and frontal thrusts, Integrated Ocean Drilling Program Expedition 316 Preliminary Report.* Washington, DC: Integrated Ocean Drilling Program Management International, Inc. doi: 10.2204/iodp.pr.316.2008

Kinoshita, M., Tobin, H., Ashi, J., Kimura, G., Lallemant, S., Screaton, E., … the Expedition 314/315/316 Scientists (2009). *Proceedings of the integrated ocean drilling program* (Vol. 314/315/316). Integrated Ocean Drilling Program Management International, Inc.

Klevtsov, D. P., Logvinenko, V. A., Zolotovskii, B. P., Krivoruchko, O. P., & Buyanov, R. A. (1988). Kinetics of kaolinite dehydration and its dependence on mechanochemical activation. *Journal of Thermal Analysis*, *33*(2), 531–535. doi: 10.1007/BF01913933

Kuo, L.-W., Song, S.-R., Huang, L., Yeh, E.-C., & Chen, H.-F. (2011). Temperature estimates of coseismic heating in clay-rich fault gouges, the Chelungpu fault zones, Taiwan. *Tectonophysics*, *502*(3–4), 293–307. doi: 10.1016/j.tecto.2011.02.001

Kuo, L.-W., Song, S.-R., Yeh, E.-C., & Chen, H.-F. (2009). Clay mineral anomalies in the fault zone of the Chelungpu Fault, Taiwan, and their implications. *Geophysical Research Letters*, *36*(18), L18306. doi: 10.1029/2009GL039269

Lachenbruch, A. H. (1980). Frictional heating, fluid pressure, and the resistance to fault motion. *Journal of Geophysical Research*, *85*(B11), 6097–6112. doi: 10.1029/JB085iB11p06097

Lachenbruch, A. H. (1986). *Simple models for the estimation and measurement of frictional heating by an earthquake, United States Geological Survey Open-File Report* (No. 86-508).

Lanson, B., Sakharov, B. A., Claret, F., & Drits, V. A. (2009). Diagenetic smectite-to-illite transition in clay-rich sediments: A reappraisal of X-ray diffraction results using the multi-specimen method. *American Journal of*

Science, *309*(6), 476–516. doi: 10.2475/06.2009.03

Lee, I. T., & Ogawa, Y. (1998). Bottom-current deposits in the Miocene-Pliocene Misaki Formation, Izu forearc area, Japan. *Island Arc*, *7*(3), 315–329. doi: 10.1111/j.1440-1738.1998.00192.x

Levy, J. H., & Hurst, H. J. (1993). Kinetics of dehydroxylation, in nitrogen and water vapour, of kaolinite and smectite from Australian Tertiary oil shales. *Fuel*, *72*(6), 873–877. doi: 10.1016/0016-2361(93)90095-J

Ma, K.-F., Tanaka, H., Song, S.-R., Wang, C.-Y., Hung, J.-H., Tsai, Y.-B., … Wu, H.-Y. (2006). Slip zone and energetics of a large earthquake from the Taiwan Chelungpu-fault Drilling Project. *Nature*, *444*(7118), 473–476. doi: 10.1038/nature05253

Mishima, T., Hirono, T., Nakamura, N., Tanikawa, W., Soh, W., & Song, S.-R. (2009). Changes to magnetic minerals caused by frictional heating during the 1999 Taiwan Chi-Chi earthquake. *Earth, Planets and Space*, *61*, 797–801. doi: 10.1186/BF03353185

Mishima, T., Hirono, T., Soh, W., & Song, S.-R. (2006). Thermal history estimation of the Taiwan Chelungpu fault using rock-magnetic methods. *Geophysical Research Letters*, *33*(23), L23311. doi: 10.1029/2006GL028088

Moore, D. M., & Reynolds, R. C. (1997). *X-ray diffraction and the identification and analysis of clay minerals* (2nd ed.). Oxford: Oxford University Press.

Moore, G. F., Bangs, N. L., Taira, A., Kuramoto, S., Pangborn, E., & Tobin, H. J. (2007). Three-Dimensional Splay Fault Geometry and Implications for Tsunami Generation. *Science*, *318*(5853), 1128–1131. doi: 10.1126/science.1147195

Moore, G. F., Park, J.-O., Bangs, N. L., Gulick, S. P., Tobin, H. J., Nakamura, Y., … Taira, A. (2009). Structural and seismic stratigraphic framework of the NanTroSEIZE Stage 1 transect. In M. Kinoshita et al. (Eds.), *Proceedings of the integrated ocean drilling program* (Vol. 314/315/316). Washington, DC: Integrated Ocean Drilling Program Management International, Inc. doi: 10.2204/iodp.proc.314315316.102.2009

Mukoyoshi, H., Kaneki, S., & Hirono, T. (2018). Slip parameters on major thrusts

at a convergent plate boundary: regional heterogeneity of potential slip distance at the shallow portion of the subducting plate. *Earth, Planets and Space*, *70*, 36. doi: 10.1186/s40623-018-0810-z

Mukoyoshi, H., Sakaguchi, A., Otsuki, K., Hirono, T., & Soh, W. (2006). Co-seismic frictional melting along an out-of-sequence thrust in the Shimanto accretionary complex. Implications on the tsunamigenic potential of splay faults in modern subduction zones. *Earth and Planetary Science Letters*, *245*(1-2), 330–343. doi: 10.1016/j.epsl.2006.02.039

Murray, P., & White, J. (1949). Kinetics of the thermal dehydration of clays. *Transactions of the British Ceramic Society*, *48*, 187–206.

Murray, P., & White, J. (1955). Kinetics of clay dehydration. *Clay Minerals*, *2*(13), 255–264. doi: 10.1180/claymin.1955.002.13.07

Nadeau, P. H., Wilson, M. J., McHardy, W. J., & Tait, J. M. (1985). The conversion of smectite to illite during diagenesis: Evidence from some illitic clays from bentonites and sandstones. *Mineralogical Magazine*, *49*(352), 393–400. doi: 10.1180/minmag.1985.049.352.10

O'Hara, K. (2004). Paleo-stress estimates on ancient seismogenic faults based on frictional heating of coal. *Geophysical Research Letters*, *31*(3), L03601. doi: 10.1029/2003GL018890

Ortega, A., MacÍas, M., & Gotor, F. J. (2010). The multistep nature of the kaolinite dehydroxylation: Kinetics and mechanism. *Journal of the American Ceramic Society*, *93*(1), 197–203. doi: 10.1111/j.1551-2916.2009.03328.x

Ozawa, T. (1965). A new method of analyzing thermogravimetric data. *Bulletin of the Chemical Society of Japan*, *38*(11), 1881–1886. doi: 10.1246/bcsj.38.1881

Ozawa, T. (1970). Kinetic analysis of derivative curves in thermal analysis. *Journal of Thermal Analysis*, *2*(3), 301–324. doi: 10.1007/BF01911411

Ozawa, T. (1986). Applicability of Friedman plot. *Journal of Thermal Analysis*, *31*(3), 547–551. doi: 10.1007/BF01914230

Park, J.-O., Tsuru, T., Kodaira, S., Cummins, P. R., & Kaneda, Y. (2002). Splay fault branching along the Nankai subduction zone. *Science*, *297*(5584), 1157–1160. doi: 10.1126/science.1074111

Pérez-Maqueda, L. A., Blanes, J. M., Pascual, J., & Pérez-Rodríguez, J. L. (2004). The influence of sonication on the thermal behavior of muscovite and biotite. *Journal of the European Ceramic Society*, *24*(9), 2793–2801. doi: 10.1016/j.jeurceramsoc.2003.10.002

Perry, E., & Hower, J. (1970). Burial diagenesis in Gulf Coast pelitic sediments. *Clays and Clay Minerals*, *18*(3), 165–177. doi: 10.1346/CCMN.1970.0180306

Petschick, R. (2010). *Macdiff 4.2.6.* Retrieved from http://www.geol-pal.uni-frankfurt.de/Staff/Homepages/Petschick/classicsoftware.html.

Polissar, P. J., Savage, H. M., & Brodsky, E. E. (2011). Extractable organic material in fault zones as a tool to investigate frictional stress. *Earth and Planetary Science Letters*, *311*(3-4), 439–447. doi: 10.1016/j.epsl.2011.09.004

Post, J. L., & Plummer, C. C. (1972). The chlorite series of Flagstaff Hill area, California: A preliminary investigation. *Clays and Clay Minerals*, *20*(5), 271–283. doi: 10.1346/CCMN.1972.0200504

Pruett, R. J., & Webb, H. L. (1993). Sampling and analysis of Kga-1B well-crystallized kaolin source clay. *Clays and Clay Minerals*, *41*(4), 514–519. doi: 10.1346/CCMN.1993.0410411

Ptáček, P., Opravil, T., Šoukal, F., Wasserbauer, J., Másilko, J., & Baráček, J. (2013). The influence of structure order on the kinetics of dehydroxylation of kaolinite. *Journal of the European Ceramic Society*, *33*(13–14), 2793–2799. doi: 10.1016/j.jeurceramsoc.2013.04.033

Pytte, A. M., & Reynolds, R. C. (1989). The thermal transformation of smectite to illite. In N. D. Naeser & T. H. McCulloh (Eds.), *The thermal history of sedimentary basins* (pp. 133–140). New York: Springer-Verlag.

Rabinowitz, H. S., Polissar, P. J., & Savage, H. M. (2017). Reaction kinetics of alkenone and *n*-alkane thermal alteration at seismic timescales. *Geochemistry, Geophysics, Geosystems*, *18*(1), 204–219. doi: 10.1002/2016GC006553

Reynolds, R. C. (1980). Interstratified clay minerals. In G. W. Brindley & G. Brown (Eds.), *Crystal structures of clay minerals and their x-ray identification* (pp. 249–303). London: Mineralogical Society.

Roberson, H. E., & Lahann, R. W. (1981). Smectite to illite conversion rates: Effects

of solution chemistry. *Clays and Clay Minerals*, *29*(2), 129–135. doi: 10.1346/CCMN.1981.0290207

Rowe, C. D., & Griffith, W. A. (2015). Do faults preserve a record of seismic slip: A second opinion. *Journal of Structural Geology*, *78*, 1–26. doi: 10.1016/j.jsg.2015.06.006

Rowe, C. D., Moore, J. C., Meneghini, F., & McKeirnan, A. W. (2005). Large-scale pseudotachylytes and fluidized cataclasites from an ancient subduction thrust fault. *Geology*, *33*(12), 937–940. doi: 10.1130/G21856.1

Saffer, D. M., & McKiernan, A. W. (2009). Evaluation of in situ smectite dehydration as a pore water freshening mechanism in the Nankai Trough, offshore southwest Japan. *Geochemistry, Geophysics, Geosystems*, *10*(2), Q02010. doi: 10.1029/2008GC002226

Saffer, D. M., Underwood, M. B., & McKiernan, A. W. (2008). Evaluation of factors controlling smectite transformation and fluid production in subduction zones: Application to the Nankai Trough. *Island Arc*, *17*(2), 208–230. doi: 10.1111/j.1440-1738.2008.00614.x

Sakaguchi, A., Chester, F., Curewitz, D., Fabbri, O., Goldsby, D., Kimura, G., … Yamaguchi, A. (2011). Seismic slip propagation to the updip end of plate boundary subduction interface faults: Vitrinite reflectance geothermometry on Integrated Ocean Drilling Program NanTro SEIZE cores. *Geology*, *39*(4), 395–398. doi: 10.1130/G31642.1

Sakaguchi, A., Yanagihara, A., Ujiie, K., Tanaka, H., & Kameyama, M. (2007). Thermal maturity of a fold–thrust belt based on vitrinite reflectance analysis in the Western Foothills complex, western Taiwan. *Tectonophysics*, *443*(3–4), 220–232. doi: 10.1016/j.tecto.2007.01.017

Sánchez-Soto, P. J., Jiménez de Haro, M. C., Pérez-Maqueda, L. A., Varona, I., & Pérez-Rodríguez, J. L. (2000). Effects of dry grinding on the structural changes of kaolinite powders. *Journal of the American Ceramic Society*, *83*(7), 1649–1657. doi: 10.1111/j.1151-2916.2000.tb01444.x

Savage, H. M., Polissar, P. J., Sheppard, R., Rowe, C. D., & Brodsky, E. E. (2014). Biomarkers heat up during earthquakes: New evidence of seismic slip in the

rock record. *Geology*, *42*(2), 99–102. doi: 10.1130/G34901.1

Scholz, C. H. (1980). Shear heating and the state of stress on faults. *Journal of Geophysical Research*, *85*(B11), 6174–6184. doi: 10.1029/JB085iB11p06174

Seno, T., Stein, S., & Gripp, A. E. (1993). A model for the motion of the Philippine Sea Plate consistent with NUVEL-1 and geological data. *Journal of Geophysical Research: Solid Earth*, *98*(B10), 17941–17948. doi: 10.1029/93JB00782

Šesták, J., & Berggren, G. (1971). Study of the kinetics of the mechanism of solid-state reactions at increasing temperatures. *Thermochimica Acta*, *3*(1), 1–12. doi: 10.1016/0040-6031(71)85051-7

Sheppard, R. E., Polissar, P. J., & Savage, H. M. (2015). Organic thermal maturity as a proxy for frictional fault heating: Experimental constraints on methylphenanthrene kinetics at earthquake timescales. *Geochimica et Cosmochimica Acta*, *151*, 103–116. doi: 10.1016/j.gca.2014.11.020

Shirozu, H. (1969). Chlorite minerals. In S. Iwao et al. (Eds.), *The clays of japan* (pp. 183–194). Tokyo: Geological survey of Japan.

Shirozu, H. (1978a). Chlorite minerals. In T. Sudo & S. Shimoda (Eds.), *Clays and clay minerals in japan, developments in sedimentology* (Vol. 26, pp. 243–264). Tokyo/Amsterdam: Kodansha/Elsevier.

Shirozu, H. (1978b). Wall rock alteration of kuroko deposits. In T. Sudo & S. Shimoda (Eds.), *Clays and clay minerals in japan, developments in sedimentology* (Vol. 26, pp. 127–145). Tokyo/Amsterdam: Kodansha/Elsevier.

Sibson, R. H. (1975). Generation of pseudotachylyte by ancient seismic faulting. *Geophysical Journal International*, *43*(3), 775–794. doi: 10.1111/j.1365-246X.1975.tb06195.x

Sibson, R. H. (1977). Fault rocks and fault mechanisms. *Journal of the Geological Society*, *133*(3), 191–213. doi: 10.1144/gsjgs.133.3.0191

Smykatz-Kloss, W. (1974). *Differential thermal analysis. application and results in mineralogy. minerals and rocks* (Vol. 11). Berlin: Springer-Verlag.

Soh, W., Pickering, K. T., Taira, A., & Tokuyama, H. (1991). Basin evolution in the arc-arc Izu Collision Zone, Mio-Pliocene Miura Group, central Japan. *Journal*

of the Geological Society, *148*(2), 317–330. doi: 10.1144/gsjgs.148.2.0317

Soh, W., Taira, A., Ogawa, Y., Taniguchi, H., Pickering, K. T., & Stow, D. A. (1989). Submarine depositional processes for volcaniclastic sediments in the Mio-Pliocene Misaki Formation, Miura Group, central Japan. In A. Taira & F. Masuda (Eds.), *Sedimentary facies in the active plate margin* (pp. 619–630). Tokyo: Terra Scientific Publishing Company.

Środoń, J., Eberl, D. D., & Drits, V. A. (2000). Evolution of fundamental-particle size during illitization of smectite and implications for reaction mechanism. *Clays and Clay Minerals*, *48*(4), 446–458. doi: 10.1346/CCMN.2000.0480405

Sugiyama, K., Filio, J. M., Saito, F., & Waseda, Y. (1994). Structural change of kaolinite and pyrophyllite induced by dry grinding. *Mineralogical Journal*, *17*(1), 28–41. doi: 10.2465/minerj.17.28

Takahashi, M., Mizoguchi, K., & Masuda, K. (2009). Potential of phyllosilicate dehydration and dehydroxylation reactions to trigger earthquakes. *Journal of Geophysical Research*, *114*(B2), B02207. doi: 10.1029/2008JB005630

Touloukian, Y. S., Kirby, R. K., Taylor, E. R., & Lee, T. Y. R. (1977). *Thermal expansion–nonmetallic solids. thermophysical properties of matter–the tprc data series* (Vol. 13). New York: IFI/Plenum.

Tsutsumi, A., Fabbri, O., Karpoff, A. M., Ujiie, K., & Tsujimoto, A. (2011). Friction velocity dependence of clay-rich fault material along a megasplay fault in the Nankai subduction zone at intermediate to high velocities. *Geophysical Research Letters*, *38*(19), L19301. doi: 10.1029/2011GL049314

Tsuzuki, Y., & Nagasawa, K. (1957). Differential thermal analysis curves for clay minerals as related to the kinetics of their dehydration. *The Journal of Earth Sciences Nagoya University*, *5*(2), 153–182.

Ujiie, K., Yamaguchi, H., Sakaguchi, A., & Toh, S. (2007). Pseudotachylytes in an ancient accretionary complex and implications for melt lubrication during subduction zone earthquakes. *Journal of Structural Geology*, *29*(4), 599–613. doi: 10.1016/j.jsg.2006.10.012

Velde, B., & Vasseur, G. (1992). Estimation of the diagenetic smectite to illite transformation in time-temperature space. *American Mineralogist*, *77*(9–10),

967–976.

Villiéras, F., Yvon, J., Cases, J. M., de Donato, P., Lhote, F., & Baeza, R. (1994). Development of microporosity in clinochlore upon heating. *Clays and Clay Minerals*, *42*(6), 679–688. doi: 10.1346/CCMN.1994.0420604

Villiéras, F., Yvon, J., François, M., Cases, J. M., Lhote, F., & Uriot, J.-P. (1993). Micropore formation due to thermal decomposition of hydroxide layer of Mg-chlorites: interactions with water. *Applied Clay Science*, *8*(2-3), 147–168. doi: 10.1016/0169-1317(93)90034-X

Vrolijk, P., & van der Pluijm, B. A. (1999). Clay gouge. *Journal of Structural Geology*, *21*(8–9), 1039–1048. doi: 10.1016/S0191-8141(99)00103-0

Weir, A. H., Ormerod, E. C., & El Mansey, I. M. I. (1975). Clay mineralogy of sediments of the western Nile Delta. *Clay Minerals*, *10*(5), 369–386. doi: 10.1180/claymin.1975.010.5.04

Whitney, G., & Northrop, H. R. (1988). Experimental investigation of the smectite to illite reaction: Dual reaction mechanisms and oxygen-isotope systematics. *American Mineralogist*, *73*(1–2), 77–90.

Yamaguchi, A., Ishikawa, T., Kato, Y., Nozaki, T., Meneghini, F., Rowe, C. D., … Kimura, G. (2014). Fluid-rock interaction recorded in black fault rocks in the Kodiak accretionary complex, Alaska. *Earth, Planets and Space*, *66*, 58. doi: 10.1186/1880-5981-66-58

Yamaguchi, A., Sakaguchi, A., Sakamoto, T., Iijima, K., Kameda, J., Kimura, G., … Curewitz, D. (2011). Progressive illitization in fault gouge caused by seismic slip propagation along a megasplay fault in the Nankai Trough. *Geology*, *39*(11), 995–998. doi: 10.1130/G32038.1

Yamamoto, Y. (2006). Systematic variation of shear-induced physical properties and fabrics in the Miura–Boso accretionary prism: The earliest processes during off-scraping. *Earth and Planetary Science Letters*, *244*(1–2), 270–284. doi: 10.1016/j.epsl.2006.01.049

Yamamoto, Y., Hamada, Y., Kamiya, N., Ojima, T., Chiyonobu, S., & Saito, S. (2017). Geothermal structure of the Miura–Boso plate subduction margin, central Japan. *Tectonophysics*, *710–711*, 81–87. doi: 10.1016/j.tecto.2016.11.004

Yamamoto, Y., & Kawakami, S. (2005). Rapid tectonics of the Late Miocene Boso accretionary prism related to the Izu-Bonin arc collision. *Island Arc*, *14*(2), 178–198. doi: 10.1111/j.1440-1738.2005.00463.x

Yamamoto, Y., Mukoyoshi, H., & Ogawa, Y. (2005). Structural characteristics of shallowly buried accretionary prism: Rapidly uplifted Neogene accreted sediments on the Miura-Boso Peninsula, central Japan. *Tectonics*, *24*(5), TC5008. doi: 10.1029/2005TC001823

Zhan, W., & Guggenheim, S. (1995). The dehydroxylation of chlorite and the formation of topotactic product phases. *Clays and Clay Minerals*, *43*(5), 622–629. doi: 10.1346/CCMN.1995.0430512

List of publications

1. Masumoto, H., Kameda, J., Arima, H., Sugiyama, K., Nagai, T., & Yamamoto, Y. (2018). Dehydroxylation kinetics of clay minerals and its application to friction heating along an imbricate thrust in an accretionary prism. *Geochemistry, Geophysics, Geosystems*, 19(9), 2991–3003. doi: 10.1029/2018GC007472

2. Hirono, T., Ishikawa, T., Masumoto, H., Kameda, J., Yabuta, H., & Mukoyoshi, H. (2014). Re-evaluation of frictional heat recorded in the dark gouge of the shallow part of a megasplay fault at the Nankai Trough. *Tectonophysics*, 626, 157–169. doi: 10.1016/j.tecto.2014.04.020

   Masumoto, H., Kameda, J., Hamada, Y., Ujiie, K., & Kitamura, Y. Lowering of the kinetic barrier of clay-mineral reactions in a seismogenic fault: Example from the Nankai subduction zone. Submitted to *Geochemistry, Geophysics, Geosystems*.